PARALLEL HYBRID KARTING VEHICLE:

MODELING AND CONTROL

by

Gülnihal Çevik

Submitted to the Graduate School of Sabancı University
in partial fulfillment of the requirements for the degree of
Master of Science

Sabancı University

August, 2012

Parallel Hybrid Karting Vehicle Modeling and Control

APPROVED BY:

Assoc. Prof. Dr. Mahmut Faruk Akşit
(Thesis Advisor) .....

Prof. Dr. Asif Şabanoviç .....

Prof. Dr. Mustafa Ünel .....

Prof. Dr. Selim Sivrioğlu .....

Assoc. Prof. Dr. Abdülkadir Balıkçı .....

DATE OF APPROVAL: .....

Parallel Hybrid Karting Vehicle Modelling and Control

Gülnihal Çevik

ME, Master's Thesis, 2012

Thesis Supervisor: Assoc. Prof. Mahmut Faruk Akşit

Keywords: Karting, Hybrid, Ultracapacitor, Lead Acid Battery, Modeling, Rule Based Control, Charge Sustaining Control, Optimal Control.

Abstract

Hybrid Electric Vehicles (HEVs) utilize energy both from internal combustion engine and an electric drive system. For an efficient energy management between two different power sources, an effective control strategy is needed. A governing algorithm is required which is developed and verified by using a lab scale plant model that is verified by sample plant simulations. An effective energy management can minimize fuel consumption and reduce emissions. The algorithm that is developed in this study consists of a finite state machine and a charge depleting control, which are mainly based on some rules and an optimal control strategy. The work involves integration of a secondary power source on an existing karting vehicle. The goal is to efficiently capture the released energy during the braking period and utilize this energy to supplement power need during acceleration. A full model of the system has been constructed using the commercially available code MATLAB/Simulink. In addition, an experimental test system has been constructed to validate modeling and simulation work. Two different power storage alternatives have been simulated and tested to determine most efficient and economically advantageous configuration. Lead acid batteries provided low cost and robustness at the expense of extra weight. Ultracapacitor storage elements have been also studied to determine level of system efficiency gains due to light weight and rapid charge/discharge characteristics at the expense of extra cost. Furthermore, their performances on different control algorithms are compared and discussed.

Paralel Hibrid Karting Aracı Modellemesi ve Kontrolü

Gülnihal Çevik

ME, Master Tezi, 2012

Tez Danışmanı: Doç. Dr. Mahmut Faruk Akşit

Anahtar Kelimeler: Karting, Hibrid, Üstün Kapasitör, Kurşun Asidi Batarya, Modelleme, Kural Tabanlı Kontrol, Şarj Devamlılıklı Kontrol, Optimum Kontrol.

Özet

Hibrid Elektrikli Vasıtalarda (HEV), enerji elektrik motoru ile içten yanmalı motor arasında paylaştırılır. Daha verimli bir enerji yönetimi için, sisteme uygun geliştirilmiş kontrol algoritması gerekir, bu kontrol algoritması da makul bir şekilde oluşturulmuş bir donanım modeli ile geliştirilip, gerçekleştirilerek doğrulanması gerekir. Etkili bir hibrid araç enerji yönetimi, akaryakıt tüketimini veya emisyonu azaltmaktadır. Bu çalışmada geliştirilecek olan kontrol algoritmaları kural tabanlı kontrol olan sonlu makine kontrol, şarj devamlılıklı kontrol ve de optimum kontroldür. Bu çalışmanın ana fikri gereğince sadece elektrik motorunun kontrolü ile geleneksel bir araç hibrid paralel araca dönüştürüleceğinden, geliştirilen kontrol algoritmaları elektrik motoru kontrolünde uygulanmaktadır. Bu çalışmada hedeflenen, frenleme anında aracın kinetik enerjisini yüksek verimle batarylarda depolayabilmek ve bu geri kazandırılabilen enerji ile sonraki hızlanma anlarında aracın gücünü destekleyebilmektir. Aracın tam bir modeli ticari olarak kullanıma açık olan MATLAB/Simulink kullanılarak çıkarılmıştır. Buna ilaveten, bir test düzeneği simulasyon sonuçlarının validasyonu için kurulmuştur. Hibrid araç için gerekli batarya grubu ucuz ve dayanıklı olan kurşun asidi batarya ile yüksek enerji depolama elemanları olan üstün-kapasitör modülü seçilmiştir. Bu batarya gruplarının performansları, yukarıda verilen kontrol algoritmaları ile beraber değerlendirilip karşılaştırılmıştır.

Acknowledgements

It is a great pleasure to extend my gratitude to my thesis advisor Assoc. Prof. Dr. Mahmut Faruk Akşit for his precious guidance and excellent support. I am grateful to Prof. Dr. Asif Şabanoviç for his supervision and excellent advises throughout my Master study. I am gratefully indebted to Prof. Dr. Mustafa Ünel for his precious contributions, advises and supports. I would like to express my gratitude to Assoc. Prof. Dr. Abdülkadir Balıkçı who was abundantly helpful and offered invaluable assistance, support and guidance. I would gratefully thank to Prof. Dr. Selim Sivrioğlu for his feedbacks, advises and spending his valuable time to serve as my jury.

I would like to acknowledge the financial support provided by Sabancı University, Mechatronics Program and SDM Research and Engineering Ltd.

I would sincerely like to thank to my laboratory friends Zhenishbek Mamattegin, Tarık Edip Kurt, Edin Goluboviç, for their help and friendship throughout my Master study. I would like to thank my laboratory friends Sanem Evren, Kübra Karayağız, Mariamu Kassim Ali, Burcu Atay, Murat Ahmedov, Ahmet Selim Pehlivan and Ömer Kemal Adak for their support and friendship throughout my Master study. Also, I would like to thank to Hasan Malkoç and Ceyhun Sezenoğlu for their great support during the experiments which are conducted on Gebze Institute of Technology.

I would especially like to thank my fiencé for his love and great support.

Finally, I would like to thank my family for all their love and support throughout my life.

Contents

List of Figures

List of Tables

Nomenclature

A_f	Cross Sectional Front Area of the Vehicle
C_d	Aerodynamic Drag Coefficient
F_a	Aerodynamic Drag Force
F_c	Climbing Resistance Force
F_{aero}	Aerodynamic Drag Force
F_r	Rolling Resistance Force
$F_{traction}$	Total Traction Force
J_{front_wheel}	Front Wheel Inertia
J_{rear_wheel}	Rear Wheel Inertia
m	Total Mass of Karting Vehicle
k_t	Motor Torque Constant
m_f	Fuel Consumption
M_eff	Effective Mass
N	Normalized State of Charge
q	Position of the Vehicle
Q	Throttle Angle
Q_{th-ch}	Throttle Angle Range for Charging
Q_{th-ch}	Throttle Angle Range for Discharging
Q_{up}	Upper Limit of Throttle Angle
Q_{low}	Lower Limit of Throttle Angle

r_{front}	Front Wheel Radius
r_{rear}	Rear Wheel Radius
ρ	Mass Density of Air
t	Time
T	Temperature
T_{EM}	Electric Motor Temperature
T_{Batt}	Battery Temperature
T_{eng}	Engine Torque
T_{sensor}	Torque Sensor Measurement
T_m	Motor Torque
$T_{traction}$	Traction Torque
V_{max}	Maximum Voltage
V_{min}	Minimum Voltage
V_{OC}	Open Circuit Voltage of Ultracapacitor
$V_{vehicle}$	Vehicle Speed
w	Angular Speed of Shaft
w_{eng}	Engine Angular Speed
P_{eng}	Engine Power
P_m	Motor Power

BSFC	Break Specific Fuel Consumption
ECMS	Equivalent Consumption Minimization Strategy
FCHV	Fuel Cell Hybrid Vehicle
HEV	Hybrid Electric Vehicle
LA	Lead Acid Battery
PHEV	Plug-in Hybrid Electric Vehicle
PM	Permenant Magnet
SOC	State of Charge
SOC_{high}	Specified Maximum Range of State of Charge
SOC_{low}	Specified Minimum Range of State of Charge
UC	Ultracapacitor

Chapter I

1 Introduction

Hybrid vehicle means incorporation of two or more power resources in the drivetrain. According to type of drivetrains, hybrid vehicles can be studied in two category such as series and parallel hybrid vehicles. As one of the energy resources works as primary source, the other source supply the required acceleration when it is needed or functions as a generator on the deceleration times.

The definition of the hybrid vehicle by Ford Motor company is as follows:

> "Hybrid vehicle is a conventionally fueled and operated vehicle that has been equipped with a power train capable of implementing at least the first three of the following four hybrid functions:
>
> - Engine shutdown when power demand is zero or negative.
> - Engine down-size for improved thermal efficiency

- Regenerative braking for recovery and re-use of braking energy
- Engine-off propulsion at low power (when engine is inefficient)"

Most of the conventional vehicles are equipped with an internal combustion engine (ICE), which can use the fuel, the primary energy source. On the other hand, the electric vehicles with batteries, flywheels or super capacitors, introduce some constraints. None of the plug-in electric vehicles can continuously supply the energy as much as a hybrid electric vehicle with fuel tank in reasonably long driving distances. Besides, these plug-in electric vehicles are heavy, and battery life is another issue for them. The combination of the conventional ICE with electric motors tries to offer a solution to these problems. While HEVs yield reduced emissions, they have also disadvantages like performing less or lower acceleration rate of the vehicle. HEVs also require maintenance service more often with respect to a conventional vehicle, since battery life is limited in addition to maintenance of the ICE and electric motor. The stability of the system is an another important issue which should be paid attention in the design of a hybrid vehicle. Even under unexpected conditions hybrid electric vehicle should allow the

driver drive safely.

In a conventional car, vehicles kinetic energy is dissipated as heat through the Brakes during deceleration. Hybrid electric vehicles recapture some of this energy by operating the electric motor as a generator. This allows the recovered energy to be gathered in batteries for further use. This is called regenerative breaking which yields power savings and reduction emissions. Different types of energy source combinations has been developed so far. While Honda developed a parallel hybrid car labeled as Honda Insight, Toyota has developed series hybrid labeled as Toyata Prius. Besides these developments, fuel cell hybrid vehicle models may compete with conventional ICE driven cars in near future.

In this study, it is aimed to utilize the regenerative brake energy efficiently, and boost of the tractive effort of the vehicle in the acceleration time intervals as a part of a fuel minimization problem. Acceleration, deceleration and transient states are analyzed, as the power usage levels differ between them. Since the temperature increase above an acceptable range effects the battery life negatively, in order to slow down the battery aging process, temperature increase in batteries is also controlled

within some limits.

1.1 Main Issues of Hybrid Vehicles

Critical point in hybrid electric vehicle design is management of batteries and electrical motors. In plug-in electrical vehicles, battery size and cost, recharging times constitute the main problems for the vehicle. Therefore, series and parallel hybrid vehicles are more preferable. Limited life of batteries pose problems in design of hybrid cars with big batteries.

The tests in Toronto showed that hybrid vehicles failed to meet the expected 20 to 30 percent fuel savings [1]. The data showed only 10 percent fuel savings could be realized. While the hybrid vehicles are most efficient in the stop and go city traffic, it is not realistic or possible to follow such a route continuously during the course of a typical journey. Therefore, cost-energy saving comparisons should be done for different driving conditions before making a decision on the type of hybrid vehicle.

While a hybrid vehicle is fueled by gasoline and use battery, an electric vehicle uses only electric motor to power the vehicle. Initially, electric vehicles were not adopted largely because of limited driving range before needing a recharge and

long recharging times. The other reason that hybrid vehicle did not become popular is that automakers did not have tendency to produce and market these vehicles. As battery technology is developing, energy storage improves and battery cost reduces. Therefore, more manufacturers are expected to focus on electric and hybrid electric vehicles.

1.2 Thesis Objectives

Electric vehicles are considered beneficial to environment in several aspects. First of all, they have higher efficiency when compared to conventional combustion engine vehicles. Carbon dioxide production from an electric vehicle is typically one-half to one-third of that of a conventional combustion engine vehicle. Furthermore, electric vehicles do not release almost any air pollutants to the environment in which they work. Third, electric vehicles typically have less noise pollution as compared to conventional internal combustion engine vehicles. They do not emit pollutants such as nitrogen oxides, volatile organic compounds and atmospheric particulate matters. The other aspect that can be considered as advantage of hybrid electric vehicle is that they do not need much oxygen unlike vehicles which have

internal combustion engine only.

Nowadays, hybrid buses are in rising trend in most of the countries. While, new buses are mostly designed as hybrid electric vehicles, in Istanbul and other cities of Turkey, conventional city buses are still common. In Istanbul city, there are approximately 2600 city buses, among them 50 buses are hybrid [2]. Conventional city buses are economical burden with their fuel consumption. Their emissions of NOx and CO_2 pose danger to cities.

At the beginning of this work, aim was to study conversion of a conventional city bus into parallel hybrid vehicle. However, due to high prototyping costs, it has been decided to start with a smaller vehicle with an internal combustion engine. Therefore, conversion of a conventional karting vehicle to the hybrid karting vehicle has been decided as focus of this study. Karting vehicle's relatively small size and simple drive train make it easier to implement a hybrid conversion. Its small size also makes it possible to construct the full-scale laboratory prototype and conduct model validation and system calibration tests. However, eventual goal of the study is to develop a sample system to be used in city busses.

While serial hybrid vehicles supply all the power by electrical motors in most recent designs, in this work electrical motor will be functioning as additional torque supply in addition to engine torque. The electric motor will be directly attached to the drive train from ICE to wheels. The main objective with electric motor addition is boosting the vehicle power when desired power is high where ICE efficiency is low while capturing energy when car is decelerating through regenerative breaking. This way, electric motor can be used to help drive the vehicle where internal combustion engine works more efficiently.

Figure 1.1: Conventional karting car

The vehicle drive modes can be categorized as: starting/accelerating, cruising, passing and regenerative braking modes. In the starting/accelerating mode of the car, a bad fuel mix or the lack

of spark can be observed which leads to exhaust of unburned fuel which also includes carbon monoxide (CO). Boost of vehicle power via motor power will reduce the emission of unburned fuel.

In the cruising mode of the vehicle, since the vehicle is not accelerating or using a very little power, some of the engine power can be used to charge the batteries. This energy can be used again during starting/accelerating and passing modes of the vehicle. While the vehicle is accelerating in these mode, the additional power supplied by electrical motor boosts the vehicle power in addition to engine power. By this mechanism, engine power is intended to be worked at its optimum fuel consumption points.

During the regenerative breaking, the kinetic energy of the vehicle is captured and stored in batteries by functioning the electrical motor as a generator. When the breaking action is applied, the hybrid control unit informs the electrical motor to work inversely as a generator. The generator output is supplied to the electrical load, so the transfer of energy to the load provides braking effect. This energy is stored in the batteries for further uses.

A typical karting vehicle requires only 2-3 kW power. In the parallel hybrid system that is subject of this study, 10-20% boost power is considered to be supplemented via an electric motor. Therefore, an electric motor with 1 kW power has been chosen to be integrated on karting vehicle drive system.

The decision mechanism to engage and manage electrical motor is controlled with a hybrid control unit. This unit serves as intermediary between data feeds and electric motor. Vehicle's speed, acceleration, fuel consumption etc kind of information is read from the electric control unit (ECU) of the vehicle via a read unit. The information that comes from the ECU is evaluated in hybrid control unit with other information coming from the battery unit. According to the vehicle speed, battery state of charge condition and the temperature of battery and motor, the desired motor speed is determined. Integrated control algorithms that are studied in the model are rule based algorithm, charge sustaining control algorithm and optimal control algorithm. For the battery package, lead acid battery group and ultracapacitor modules are studied. These two battery units show differences in terms of their energy storage capabilities, size, price and performance on energy delivery. Performance of

different control algorithms with different system combinations have been studied and through actual simulations in a laboratory test bench system.

1.3 Contribution of This Work

- A hybrid karting vehicle mathematical model has been developed. Then, the model is tested on Simulink/Matlab with the usage of Simscape/Mechanical Library.

- Lead acid battery and ultracapacitor models have been integrated into the system model with their internal resistance and temperature models.

- Three different control algorithms have been developed: rule based control algorithm, charge sustaining control algorithm and optimal control strategy based on fuel minimization on the constraint of no change in the state of charge of the battery at the end of the driving cycle.

- The developed control algorithms have been simulated with ultracapacitor and lead acid battery groups separately, while battery performances are evaluated with developed control algorithms.

- A prototype system model has been constructed in laboratuary environment. Developed control algorithms have been applied with both lead acid battery and ultracapaci-

tor modules in laboratory environment, and their efficiencies have been calculated.

Chapter II

2 Literature Survey on Hybrid Electric Vehicles, HEV Components and HEV Control Strategies

2.1 Hybrid Electric Vehicle Types

HEVs use regenerative brake energy efficiently by converting kinetic energy into electric energy which is stored in batteries instead of being wasted as heat dissipation through the brake disks. Furthermore, many hybrid electric vehicles reduce idle emission by stoping the ICE at idle time intervals. Some hybrid electric vehicles use internal combustion engines to generate energy directly either to store the energy in the batteries for further use through electrical motor, or to use it directly by the electrical motor to supply drive power. On the other hand, in

some hybrid electrical vehicle models, internal combustion engine and electric motor share the traction effort to make the internal combustion engine work at its efficient region to reduce the fuel consumption.

Hybrid vehicles can be categorized by how they power a vehicle. One can categorize hybrid vehicles as parallel hybrid electric vehicles, series hybrid electric vehicle and power split hybrids which have the characteristics of both parallel and series hybrid vehicles. While the series hybrid is efficient at lower speeds, parallel hybrid is efficient at higher speeds, and power split vehicles can benefit both efficiently. On the other hand, plug-in hybrid vehicles also exist which use the battery stored energy which is charged by a plug while also having ICE to generate energy in order to fill the batteries on the move.

It is also possible to categorize the hybrid vehicles with their fuel sources as hybrid vehicles which use fossil fuels and biofuels. Besides, fuel cell hybrid vehicle technology is developing which uses hydrogen as fuel which is zero emission technology.

2.1.1 Parallel Hybrid Electric Vehicles

In a parallel hybrid vehicle a motor and internal combustion engine power the vehicle together. The electric motor and engine is coupled with a clutch mechanism. Vehicle can be tracked purely in electric mode. While the vehicle is in the combustion engine mode, the vehicle is powered by both electric motor and the engine.

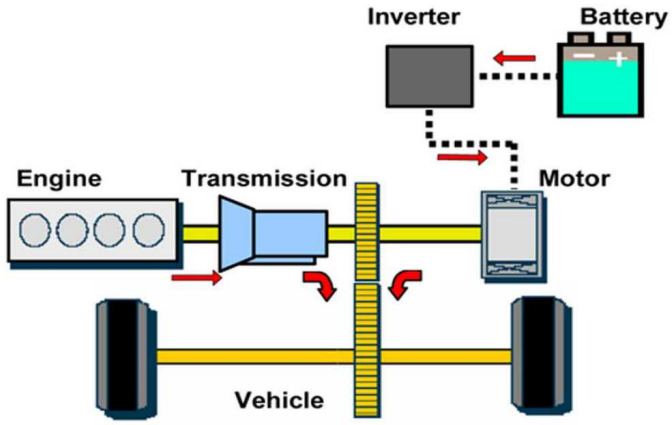

Figure 2.1: Parallel Hybrid Electric Vehicle Structure [3]

Besides powering the vehicle together, there is another kind of parallel vehicle type which is mild parallel hybrid. Mild hybrid electric vehicle has an electric motor in addition to the engine, but in this type motor stands for power assisting in the acceler-

ation mode and energy generator in the decelerating mode.

2.1.2 Series Hybrid Electric Vehicles

A series hybrid vehicle is mainly powered by the electric motors. In a series hybrid electric vehicle, a part of traction energy is converted into electrical energy and then into the mechanical energy and some part of the energy is directly sent to the wheels via mechanical transmission. Series hybrid vehicle configuration has the higher overall efficiency. Moreover, the pure electrical output offers higher flexibility to control the power and reduced noise output.

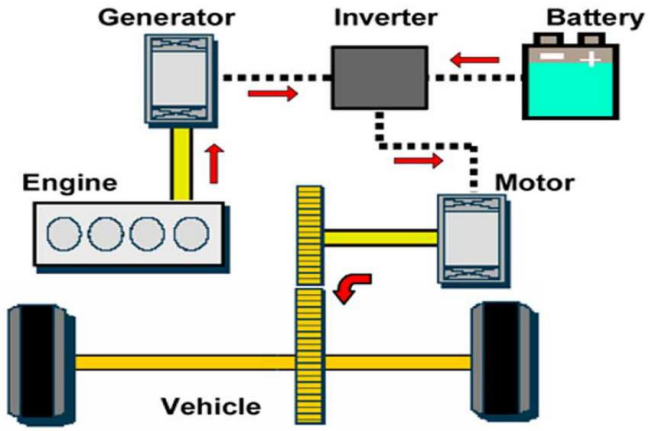

Figure 2.2: Series Hybrid Electric Vehicle Structure [3]

There is another kind of parallel hybrid vehicle type which is called mild parallel hybrid. Mild hybrid electric vehicle has an electric motor in addition to an IC engine. However, in this type, motor is used for power assisting in the acceleration mode, and acts as electric energy generator in the decelerating mode.

2.1.3 Plug-in Hybrid Electric Vehicles

An plug-in electric vehicle is powered by electric motor instead of a gasoline engine. Energy which is necessary for the electric motor is controlled by a controller. Controller regulates the amount of power based on the accelerator pedal position that a driver applies. Energy is stored in rechargeable batteries that can be charged by common household electricity.

In series and parallel hybrid vehicles, initial condition of the battery does not have a considerable effect on driving range. However, in plug-in hybrid electric vehicles (PHEV), mainly existing battery power has been used. Therefore, battery initial state of condition (SOC) and their capacity has an important effect on the driving range. Besides, while the trip length and initial SOC have crucial role on the determination of fuel economy, the increasing trip distance makes PHEV less economical

[4].

PHEV control strategies can be mainly divided in two categories: Blended Mode and EV Mode. EV mode can be described as charge depleting mode as far as electric motor may supply the needed power, and the SOC is above the described limit. In the blended mode, it is aimed that the SOC reaches to the lower limit at the end of the travel. This control strategy requires the priori knowledge of the road and the velocity profile.

Furthermore, ECMS (Equivalent Consumption Minimization Strategy) is an another control method for PHEVs which uses the knowledge of total energy consumption to make the local optimization while keeping SOC constant. ECMS may have three degrees of freedom which are internal combustion engine power, electric motor power and belted starter alternator power. This controller searches for optimum power share between engine and EM to minimize equivalent fuel consumption [4].

2.1.4 Fuel Cell Hybrid Electric Vehicles

For sustainable mobility, it is important to consider the other energy supplies other than the conventional ones like fossil fuels. It is also important to apprehend the CO_2 emission to atmo-

sphere. As it can be seen from the figure below, in parallel to the increase of CO_2 level, environmental problems also grow. Fuel cell hybrid vehicles (FCHV) are environmental friendly, since they do not emit CO_2. However, they also cause indirect emission level of which may vary according to the primary source of energy.

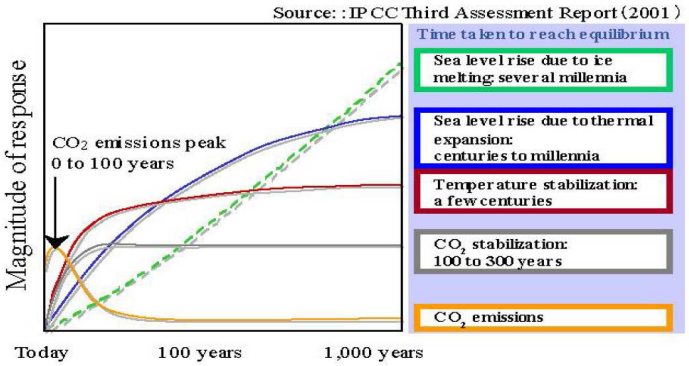

Figure 2.3: Influence of CO_2 emission [5].

One of the drawbacks of the fuel cell hybrid vehicle is that there is only a limited number of hydrogen stations [5]. It is also hard to get sufficient fuel tank capacity for a range of 500 km [5]. Besides, in the cold weather conditions, freezing is an inevitable phenomena. Considering all these conditions, more research and developments are required to see the FCHVs on

roads.

2.2 Proposed System

The proposed hybrid karting vehicle can be called as parallel hybrid karting, since the primary power source is internal combustion engine and the secondary power source is battery powered electric motor. A karting vehicle is converted to the hybrid karting vehicle with an electric motor coupling extension to the engine shaft. The electric motor boosts the power during the acceleration time intervals and functions as power generator in the deceleration time intervals. Besides, the electric motor may help the engine by sharing the power or functioning as generator in order to fill the batteries on lower SOC conditions, on cruising time intervals.

2.3 Electrical Motor

In this work, as an electric motor of the hybrid karting vehicle, permanent magnet (PM) motor has been chosen with its generator characteristic. PM DC electric motor has the following benefits [6]:

- " Higher efficiency since no electrical energy is used or losses

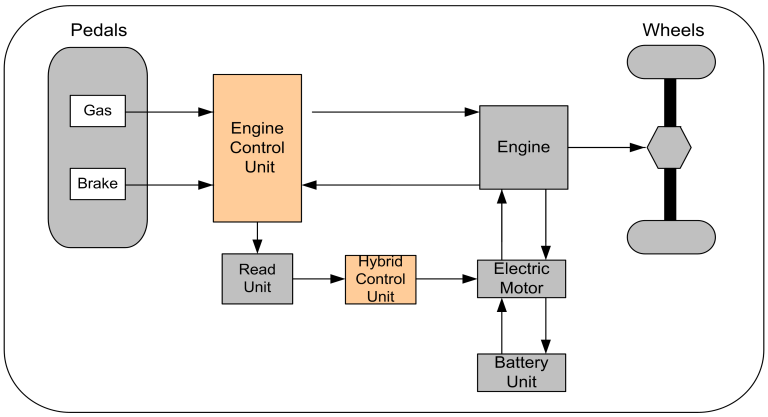

Figure 2.4: Proposed Hybrid Karting Vehicle Diagram

incurred for developing or maintaining the motor's magnetic field.

- Higher torque and power density.
- Linear torque speed characteristics that are more predictable.
- Better dynamic performance due to higher magnetic flux density in air gap.
- Better dynamic performance due to higher magnetic flux density in air gap.
- Simplified construction and essentially maintenance-free. More compact size."

2.4 Battery

Hybrid vehicles have capability to recover the kinetic energy by regenerative breaking in the storage elements like ultracapacitors; lithium-ion batteries etc and reuse it in the next acceleration processes. Storage elements show difference in terms of their storage capability, charge and discharge times, and their efficiencies. Besides technical issues, their size and cost are also important to make a choice between them. In following sections, charge-discharge characteristics of storage elements are analyzed and compared with respect to their size and cost in order to provide optimum choice for a hybrid vehicle. Suitable battery/energy storage options has been studied for a karting vehicle. Then, their performance is compared through simulation and experimental results based on a given driving cycle for selected ultracapacitor and lead acid battery groups.

2.4.1 Nickel Metal Hydride batteries

Nickel metal hydride battery (NiMH) which was introduced commercially in the last decade of 20th century is a type of rechargeable battery. It resembles to nickel-cadmium battery in terms of performance, but the only difference between them

is that NiMH's negative electrode uses hydrogen. As for their capacity, NiMH battery has two or three times the capacity of an equivalent size nickel-cadmium battery.

NiMH cell chemistry hasn't had a good fame since the introduction of lithium based cell chemistries. Although there are several consumer applications in which the usage of NiMH have been completely replaced by lithium-ion, NiMH chemistry has been preferred in automotive applications. One of the main reasons why this battery is applicable in this industry is that the operation temperature range of NiMH cells has been expanded to 100 Celsius while that range of Lithium cells can not reach to this level. That is why, NiMH technology is regarded as appropriate for automotive industry.

Advantages of nickel metal hydride batteries can be explained as follows. First of all, these batteries have some benefits from environmental perspective. As the technology progresses, the electronic devices get smaller depending on batteries. Since NiMH batteries can be charged over and over again, this reusage can reduce the burden of landfills. Another advantage is that NiMH batteries have very acceptable size and weight. While other batteries are bulky and heavy, the size and weight of NiMH

batteries make them ideal for general usage.

When it comes to disadvantages of NiMH batteries, it can be said that these batteries can not work properly in higher or lower temperatures. Another issue which can be regarded as disadvantage of these batteries is that their self-discharge rates are high. They are also much intolerant to over-discharging, since this situation leads to polarity reversal which effects the battery permanently. Moreover, it can be observed frequently that NiMH batteries stop suddenly.

2.4.2 Lithium-ion batteries

Nickel cadmium batteries had been the unique suitable batteries for portable equipments for many years. Lithium-ion cells have been introduced during late 1980s. Today, lithium-ion batteries are the fastest growing and the most prominent batteries. The basic feature of these batteries is their increased energy density and accordingly increased cost when it is compared to other rechargeable batteries. These batteries can be observed in the most expensive laptops in the market because of their high prices.

The efforts to develop rechargeable lithium batteries were not

successful due to security reason. Since lithium metal had an instability especially during charging, researches started to focus on non-metallic lithium battery, that is lithium-ion batteries. Lithium-ion batteries are safe although they are slightly lower in energy density than lithium metal batteries.

One of the main advantages of lithium-ion batteries is that their low maintenance while most other chemistries can not have this property. Additionally, they do not need to have memory and scheduled cycling to prolong their lifetime. For another advantage, it can be said that self-discharge of them is less than half when compared to nickel-cadmium. That enables lithium-ion batteries to be useful for modern fuel gauge applications.

Despite its advantages, it has some disadvantages. First, lithium-ion battery is fragile and needs protection circuit to maintain safe operation. Protection circuit which is built into each pack puts a limit on zenith voltage of each cell during charge and protects the cell voltage from dropping too low level on discharge. Furthermore, the cell temperature is observed to hinder the temperature extremes.

2.4.3 Ultracapacitors

Ultracapacitors are quick chargeable storage elements which are providing a solution as high energy accumulators for hybrid vehicle power trains. Ultracapacitors are being accepted as power storage elements for many hybrid vehicle energy units. Some of the main reason are their high pulse power capability, fast transient response, and high efficiency during discharge and recharging. They also endure full charge cycling in excess of 100000 cycles [13]. However, a big challenge for the usage of ultracapacitors is the cost, since they are not being produced in massive quantities.

Ultracapacitor is true choice if the energy is desired to be stored by charge separation at the electrode-electrolyte interface. Moreover, another characteristic of it is that its strength to be able to withstand large amount of charge/discharge cycles without suffering performance loss.

Ultracapacitors are energy storage devices, and in this respect, they are similar to batteries. In order to meet the power, energy and voltage necessity, various-sized cells are designed into modules. While batteries store the charge with the help of chemical process, ultracapacitors execute this task by apply-

ing electro-statical procedure.

The working procedure of ultracapacitor can be defined as follow: Electrolytic solution is polarized by ultracapacitor so as to store the energy electrostatically. In this process, there is no observable process. This mechanism can be reversed, that is, ultracapacitor can be discharged and charged many times. An ultracapacitor is constructed by two nonreactive collectors. When the voltage is applied on the positive electrode, it attracts the negative ions; whereas when the voltage is applied on negative electrode, it makes the positive-ions closer to itself.

Energy that is stored after charging the ultracapacitor can be used by vehicle's motor. When compared to usual capacitors, the amount of stored energy very large due to extensive surface area created by the porous carbon electrodes. On the other hand, the stored energy seems to be less compared to that of batteries. The proportions of charge and discharge operations are determined by only physical properties of ultracapacitor. That is why, the ultracapacitor can release energy much faster than a battery.

Ultracapacitors can be prominent energy devices for power supply during acceleration and climbing a hill. It is possible to

use them with batteries correspondingly. In this case, the power performance of ultracapacitors and energy storage capability of batteries can be combined. Moreover, ultracapacitors are able to make the lifetime of batteries longer.

2.4.4 Lead-Acid batteries

The oldest type of rechargeable batteries is lead acid battery system. They are able to serve high surge currents and it means that cells have relatively high power-to-weight ratio although they have very low energy-to-weight ratio, and low energy-to-volume ratio. Hence, they turn out to be available for motor vehicles due to the fact that their cost is low, and they can provide high current which is necessary for automobile starter motors.

Between other battery groups lead acid batteries are abundant, therefore, their prices are low. They are also reliable, robust and tolerant to overcharging. However, charge-discharge cycles are repeated in excessive number of times in hybrid vehicles, while life cycles of lead acid batteries are limited to numbers of ~ 500. Besides, they are bulky and can not be charged quickly. Therefore, usage of lead acid batteries should be in

combinations with the batteries with higher life cycles.

Some of the main problems of lead acid batteries are sulphation, shedding and decomposition of electrolyte. (Shedding means loss of materials from the main plates). Therefore, they should be maintained regularly. Battery resistance increases with the rapid increase on current demand, which also degrades the lifetime in the long process. Battery management should be properly handled in order to take the optimum performance and the life.

2.4.5 Advantage and Disadvantage Comparison of Batteries

Battery Group	Advantages	Disadvantages
NiMH	Performs at high temperatures Small size and weight Environmently friendly	Limited temperature range High self discharge Intolerant to overdischarging
Lithium-Ion	Low maintanence High energy density Low self discharge	Fragile Expensive Instability issue on charging
Ultracapacitors	High specific power High efficiency at dis/charging High cycle rate	Low specific energy Self discharge Very Expensive
Lead Acid	Cheap Low self discharge Robust	Slow charging Limited cycle life Sulphation, shedding

Table 2.1: Battery comparison table

2.4.6 Ultracapacitor and Lead-Acid Battery Combinations

The braking energy that is recuperated through the generators can be fed into ultracapacitor modules fast. Since ultracapacitors are storage elements with low energy per unit mass, it is hard to meet the energy demand of the hybrid vehicle powertrain with the lower power density of ultracapacitors. Therefore, combination of ultracapacitors with lead acid batteries, which

have high energy per unit mass, are being used.

A DC/DC converter exists between the ultracapacitor and lead acid battery. A power flow control unit is necessary to maintain the power flow between lead-acid and ultracapacitor as well as the flow to and from the ultracapacitor in order to minimize the fuel consumption of the engine.

It is reported by the Argonne National Laboratory that lead acid batteries best fit with ultracapacitors, since the specific power deficiency of the lead acid battery can be compensated by ultracapacitors [15]. Lead acid batteries lifetime is shorter, and the combination with ultracapacitors extends their life. In a work by Stienecker et. Al [16], in order to prolong the lifetime of the lead acid battery group, SOC is kept at maximum and only in the times of high current request lead acid batteries aid the energy demand.

Baisden et. Al. [17] used capacitor and batteries in parallel since batteries can store sufficient energy but capacitors cannot. On the other hand, capacitors can supply the large burst of current ad batteries cannot. They used 35 of PC2500 Maxwell ultracapacitor (3000F - 2.7 V) and 18 of Hawker Genesis 12 V 26Ah 10EP lead acid battery combination in the simulation

environment of ADVISOR. Their results showed that UC-LA Battery combination fuel economy is 19.69% better than the conventional (non-Hybrid) vehicle and 2.41% better than the battery source used in parallel hybrid vehicle [17].

In another work by Napoli et. al. [18], the power sharing is done according to optimum share of power flow with maximum efficiency and SOC values of batteries with a rule based algorithm. Besides the choice of battery and control of them is an important issue. The DC-DC converter topology used between the LA battery and ultracapacitors is also important. In [19], ultracapacitor and battery combination is used with the topology of the two-input bi-directional DC-DC converter and compared with the passive parallel connection. Results showed that two input bi-directional DC-DC converter is more efficient and its output stability is better.

In a work by Garcia et. al. [20], the power demand has been divided into categories of low frequency components and high frequency components. While the low frequency components are supplied by the batteries, high frequency components are supplied by the ultracapacitors. In this method, it is aimed that battery life will be longer.

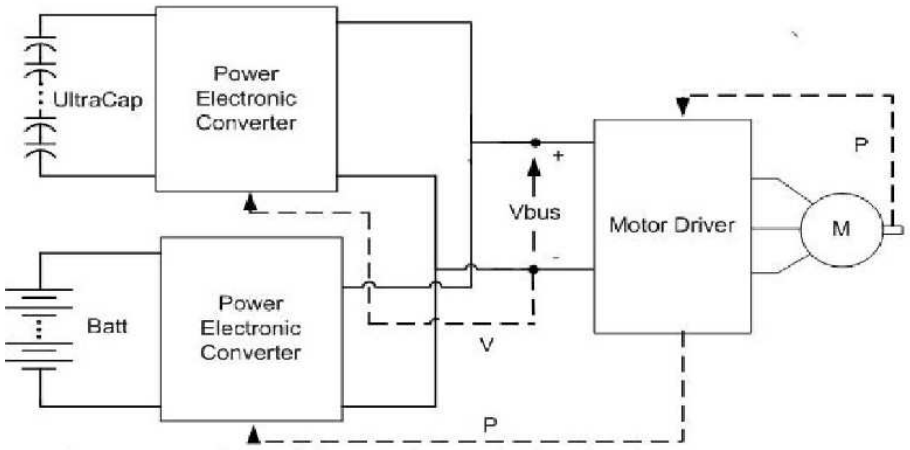

Figure 2.5: Topology of the Two-input Bi-Directional DC-DC Converter [19]

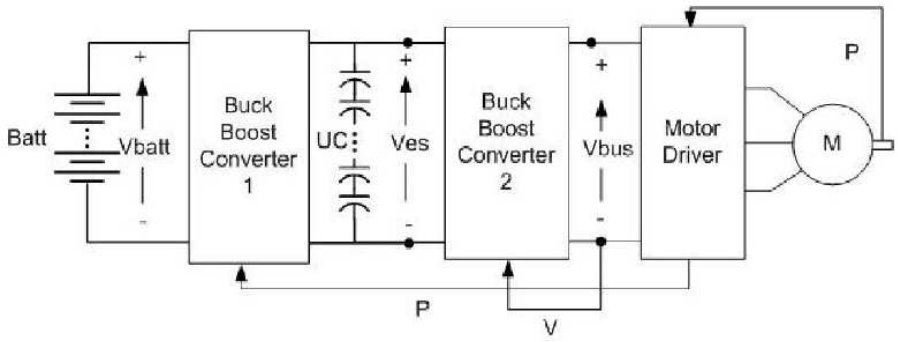

Figure 2.6: Topology of the Bi-Directional DC-DC Converter [19]

2.4.7 Comparison of Ultracapacitors

In order to use the capacitors effectively, when their voltage is decreased by half, the recharging process should be restarted. As one can see from the figure below, combinations of single

cells in series is cheaper with respect to the modules. However, problem arises with cell coordination problem. Each of the cells require voltage balancing circuits. However, these circuits solve the problem only partially. Another requirement is the isolation of the cells. Therefore, it is highly recommended to use the capacitor modules.

For a karting vehicle, it is suitable to have a 1kW motor. The available ultracapacitor cell combinations, module types, and their powers are tabulated with their estimated time to support 1kW electric motor. Initial voltage values (Vi), final

Brand	Pictures	Dimensions (mm)	Weight (kg)	Voltage	Quantity	F	Vi	Vs	Es (Wh)	estimated time for 1KW (s)	Total Price
Maxwell		418x190x110	10,5	48	1	83	48	24	19.92	24	$1,392.00
Maxwell		102x60x60	0,28	2.7	20	1500	54	24	24.375	24	$1,500.00
NESSCAP		430x200x110	11,3	48	1	88	48	24	21.12	21	$2,270.00
NESSCAP		75x60x60	0,28	2.7	20	1200	54	27	18.225	21	$1,900.00
loxus		418x150x191	15	48	1	165	48	24	39.6	48	$1.200,00
loxus		134x60x60	0,525	2.7	20	3000	54	27	45.563	48	$1,203.00

Figure 2.7: Comparison table for ultracapacitor cell and modules to work with 1kW and 2kW motors

voltage values (Vs) and the increasing resistance by usage time and system losses are considered in calculation of the time estimates. One can choose the suitable module or cell combination by considering price and estimated time to support a particular electric motor.

2.5 HEV Control Strategies

In hybrid electric vehicles, a control strategy is necessary in order to make the engine work at its efficient range. This control strategy can be based on some rules, if the driving range is not known priori. The rule based control strategy can be based on look-up tables, or can be made robust by using fuzzy logic control strategy. Moreover, HEV control can be based on optimization process. Optimization can be conducted globally, if the priori driving range and conditions are known. It can also be done in real time, if the route conditions are reachable periodically.

2.5.1 Rule Based Control Strategies

The overall aim of a rule-based (RB) control strategy is to push the ICE to the optimal region of fuel consumption and ef-

ficiency. However, this strategy is not efficient at the low engine torques and speeds [40]. Vehicle controller is based on selection of one of the five driving modes (motor alone mode, combined power mode, engine alone mode, electric CVT mode, energy recovery mode) [22]. Aim of this strategy is optimization of the engine power in different driving modes. Once the engine power is specified, the engine angular velocity can be determined by the optimum angular velocity that corresponds to desired engine power. Then, the motor torque is the complementary part to satisfy the required torque assistance [22].

2.5.1.1 Deterministic Rule Based Technics

The deterministic rule based control strategy is applied via lookup tables by considering fuel economy, ICE operating maps, power flows within the powertrain and driving experience [40]. The thermostat control cannot achieve supplication of enough power demand. On the other hand electric assist control strategy cannot achieve optimal powertrain efficiency [40].

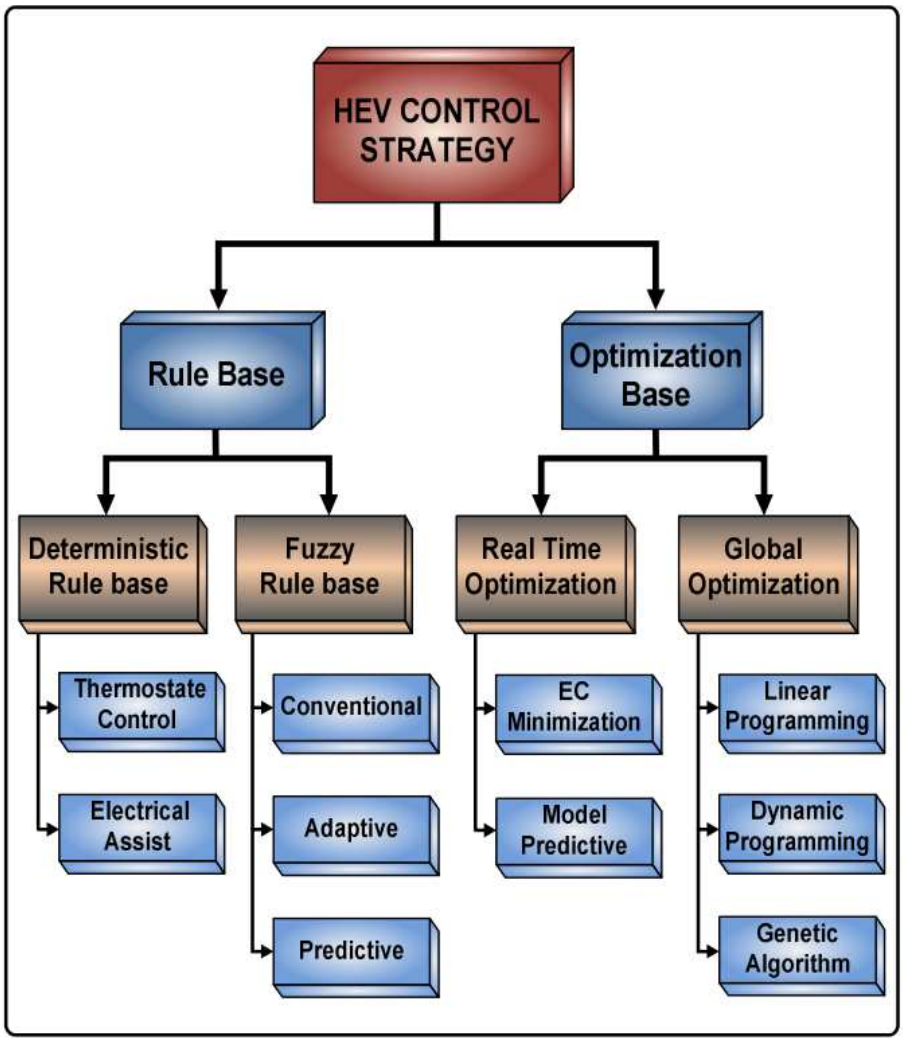

Figure 2.8: HEV Control Strategies [40]

Zhang et. al. [23] developed the charge depleting control strategy which is called as optimal power strategy that is different than electric assist mode. In the electric assist mode, electric motor engages when the road load is more than the engine opti-

mal. The concern of their study is developing control strategy in addition to the assist control. First of all, electric motor will be on working mode till the threshold power P_S is reached. Then, when the motor power is not sufficient, engine turns on to assist. A constant motor power P_c will be continuously supplied till the end of the drive cycle. Vehicle desired power has the relationship "$P_o = P_{eng} + P_{EM}$". P_c is arranged according to P_o , $P_{c_{min}}$ for optimal value by considering drive cycle and the power demand. According to proposed control strategy, engine turns off when the power demand is less than the optimal power threshold $P_{c_{opt}}$. $P_{c_{opt}}$ is determined according to system loss characteristics, vehicle power demand, total battery energy and trip distance. The proof of this optimization method is shown by the simulations. The results show that above 70 mi/h power saving is increasing. Moreover, it is shown that in the CR-City drive cycle fuel efficiency is increased by 4.2% with respect to the electric assist control strategy [23].

In a different work by Won et. al. [24], energy management of a parallel hybrid vehicle is done with the charge sustaining scheme. This is realized by the decision of torque distribution on engine and the electric motor. In their work, torque distri-

bution is formulated as a multi-objective nonlinear optimization problem and solved by the single objective linear optimization problem.

2.5.1.2 Fuzzy Rule Based Technics

Since HEVs have nonlinear and time-varying structure, fuzzy logic control strategy is suitable to handle problems of HEVs with its robust and adaptable properties [40]. Fuzzy logic controller takes battery SOC and desired ICE torque as inputs. However, it does not take into account the ICE efficiency maps. In this control strategy, ICE is operating in its efficient region. However, this efficiency leads to more torque generation than necessary, so the increase of fuel consumption [40]. Fuzzy predictive control strategy optimizes the fuel consumption with look-ahead window which gives the future road driving conditions [40]. Syed et. al. [25] used selective minimal rule-based fuzzy gain-scheduling to determine proper gains for the PI controller based on the system's operating conditions. It is noted that high-voltage battery management is critical in hybrid systems, and a conventional PI controller may result in overshoots or degraded response and settling times due to nonlinearities. The

designed minimal rule based fuzzy gains scheduling controller improved the engine speed and the power behavior in a power-split HEV.

In a work done by Tian Yi et. al. [26], fuzzy-genetic control strategy is applied on parallel hybrid vehicle power management. The experiments showed that fuzzy genetic control algorithm resulted in reduced emissions, and improved fuel consumption with respect to results with fuzzy controller. Genetic algorithm is stated for the optimization of thirty parameters in the fuzzy control law and applied on China HEV driving cycle.

In another research conducted by Lee et. al. [27], torque control strategy is applied with the fuzzy logic on parallel hybrid bus. An induction machine is directly coupled to the engine shaft. In their work, max-min composition techniques and center of gravity methods are used. Moreover, they divided the controller in two parts, driver's intention predictor (DIP) and power balance controller. The proposed design improved the driveability of vehicle, balanced the battery charge and reduced the emission.

Yifeng et. al. [28] also used the genetic-fuzzy control strategy in order to keep the SOC at a certain level by employing repro-

duction, crossover and mutation. When it is compared with the fuzzy strategy, it gives better results. Genetic algorithm is suitable for tuning the parameters in real time.

2.5.1.3 Sliding Mode Based Control

In a work done by Gokasan et. al. [29], series hybrid vehicle power train control is based on two chattering-free sliding mode controller. They achieved control of the engine speed and engine/generator torque which together leads the engine to work at its efficient regions. Engine/generator torque control with sliding mode control based strategy gives better tracking performance of speed and torque references in the optimal efficiency region. Besides, in the work of Demirci et. al. [30], optimization of auxiliary power unit (APU) is done by an offline optimum search algorithm by regarding the demanded power. Moreover, control of engine speed of APU is achieved by a chattering free sliding mode control. This algorithm revealed high set point tracking, smooth cranking, running and stopping of APU on the applied series hybrid electric vehicle.

In another work by Wang et. al. [31], a sliding mode variable structure control strategy is implemented on maximum torque

per ampere vector control system of interior permanent magnet synchronous machine (IPMSM) in order to resist against any disturbances on hybrid electric vehicle. They used improved variable exponent reaching law to reduce the chattering effect of the system.

In a separate work [32], position-sensorless electric vehicle with a brushless dc motor is studied. Implementation of electromotive force detection method allowed sensorless control of the motor. Combination of nonsingular terminal sliding mode with the higher order sliding mode method, hybrid terminal sliding mode control (HTSM) algorithm resulted with good system performance and robust stability when compared to the PID controller for EVs.

Hong Fu et. al. [33] designed a controller using DTC-SVM (Direct Torque Control-Space Vector Modulation) technique with sliding mode controller for plug-in hybrid vehicle. By this technique, fast response and small torque ripples are achieved. The claim that this control system is robust against load variations, measurement errors and parameter uncertainties.

Tian-Jun Fu et. al. [34] improved speed-sensorless torque control of an induction motor for HEVs with the principle based

on Sliding Mode Control (SMC) combined with the space vector modulation (SVM). They claim that this improves torque, flux and current steady state performance by reducing the ripple. This control model improved the accurate torque tracking and robustness is realized to external disturbances.

Cheong et. al. [36] proposed that a model reference sliding mode control which generates additional yaw moment for the vehicle. It is simulated on a 4 wheel drive (4WD) hybrid electric vehicle considering the cornering stability. In the work of Taghavipour et. al. [37], sliding mode control is designed to use full-states closed loop feedback which satisfies the stability of the vehicle in different modes.

In the study of Yim et. al [**?**], active roll control system (ARCS) and integrated chassis control (ICC) for hybrid 4WD vehicle whose rear tires are powered by the electric motor. ARCS is designed with sliding mode control. An integrated chassis control is designed to maintain the maneuverability. In ICC, weighted least square method has been integrated to define actuator configurations.

In a study by Kasahara et. al. [39], sliding mode control is applied on braking control. Optimal control is applied by

switching wheel speed following and slip ratio following on the boundary of slip ratio where the maximum braking force is acquired.

2.5.2 Optimization Based Control Strategies

2.5.2.1 Global Optimization

Genetic Algorithms are efficient, since they can find the global minima. However, these algorithms are time consuming, and do not consider the SOC situation[40]. Real time equivalent consumption minimization strategy only uses the current system parameters. No future predictions are needed, and it varies with the driving conditions. Only charge sustainability can not be supplied[40]. Another real time optimization model is model predictive control which uses the traffic information, driving pattern and route information and saves fuel[40]. On the other hand, there exist global optimization solutions which are working on fixed driving cycles. However, with this method, real time management is not possible[40]. With dynamic programming, HEV nonlinearities can be handled by minimizing cost function over a fixed driving cycle [40].

Global optimization problem for energy can be solved by min-

imizing fuel consumption or overall CO_2 emission. Stockar et. al. [41] solved the global optimization problem by minimizing CO_2 emission by Pontryagin's minimum principle.

Delprat et. al. [42] applied optimal control theory for a given driving cycle. In their study, optimal control theory is based on different battery models. Ngo et. al. [43] combined the dynamic programming and classical optimal control theory for fuel minimization over a preview route segment. The Global Positioning Systems and Geographical Information System is used to utilize route information, this leads to the fuel economy within a specified time length.

The hierarchical control strategy optimization can also be applied by the PSO (Particle Swarm Optimization) by combining the best solutions of the sections and the global best value of the whole part for fuel minimization [44]. In a study by Sciarretta et. al. [45], fuel optimization is developed without relying on priori knowledge of the future conditions. They used the instantaneous cost function, and weighting is used between two different energy source by introducing equivalence factor.

In another work, Zhang et. al. [46] optimized blended mode to study PHEV's. This optimization is done by finding the

optimum power to initiate the engine for constant battery energy depletion, below that engine work power limit, vehicle power will be sustained by the battery source.

Chapter III

3 Modeling & Control of the Parallel Hybrid Karting Vehicle

A modeling is required to see the performances of developed control strategies before they get tested on a test-bench. In order to simulate the reality, a correct model is required. In this work, model is developed by considering the vehicle mechanical system, environmental conditions like air, temperature etc, and electrical system which includes electrical motor and battery dynamical model.

Control of parallel hybrid vehicle is developed in order to enable engine to work at its efficient region by controlling the electrical motor effort. In this work, rule based control, charge sustaining control and optimal control strategies have been developed for the karting vehicle in order to compare, and find the suitable control strategy.

3.1 Parallel Hybrid Karting Vehicle Modeling

In the study of hybrid car modeling, electric motor is directly attached to the shaft of the vehicle, so the engine and the electric motor are sharing the traction power. The engine does not consider how much power should be delivered to the system by the electric motor. Therefore, engine is functioning as velocity controller by compensating the traction power.

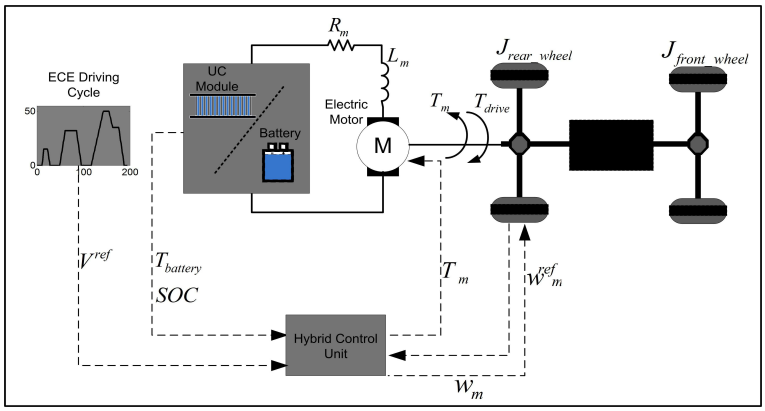

Figure 3.1: Karting vehicle model diagram

3.1.1 Tractive Effort Calculation

A vehicle has to accomplish many tasks to do its main task, going forward. Main tasks can be listed as follows

- Overcome rolling resistance.
- Overcome aerodynamic drag.

- Supply sufficient energy to accelerate the vehicle when needed.
- Overcome the climbing resistance when driving up hill.

3.1.2 Rolling Resistance Force

Rolling resistance is mainly due to the friction of the wheels with the roads. The resistance is correlated with the vehicle speed, but most of the time the variation can be neglected to be taken as a constant. Another direct factor of rolling resistance is the weight of the vehicle which affects proportionally. Yet another factor that affects rolling resistance is the wind that goes in and around the wheel space. Rolling resistance force can be described as in the following

$$F_r = \mu \cdot m \cdot g \tag{1}$$

where μ is the friction constant, m (kg/m^2) is the mass of the vehicle and g (m/s^2) is the gravitational constant. Here, rolling resistance constant can be chosen by considering the tire material, road properties and geometry.

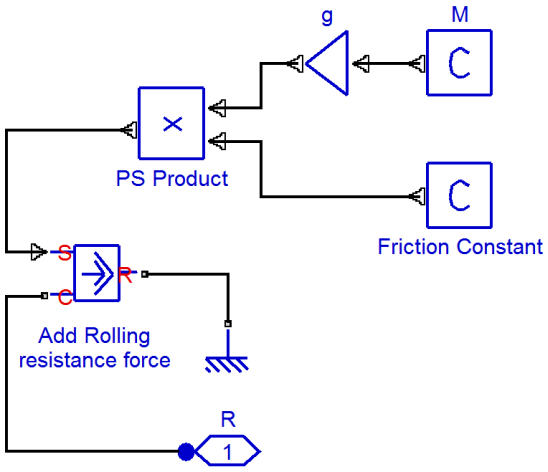

Figure 3.2: Rolling Resistance Simulink Model created by Simscape/Mechanical Library

3.1.3 Aerodynamic Drag

The aerodynamic drag force is mainly due to the friction of the vehicle body through the air. Shape and the surface material are main components that affect the aerodynamic drag. In order to describe the aerodynamic force, frontal area and shape of the vehicle should be defined well. Aerodynamic force becomes more significant in high speed ranges. The aerodynamic force can be described as in the following:

$$F_{aero} = \frac{1}{2} \cdot \rho \cdot C_d \cdot A_f \cdot V^2 \tag{2}$$

where ρ (kg/m^2) is the mass density of the air, C_d is the aerodynamic drag coefficient which can be decided according to frontal shape, A_f (m^2) is the cross sectional frontal area of the vehicle and V (m/s) is the speed of the vehicle.

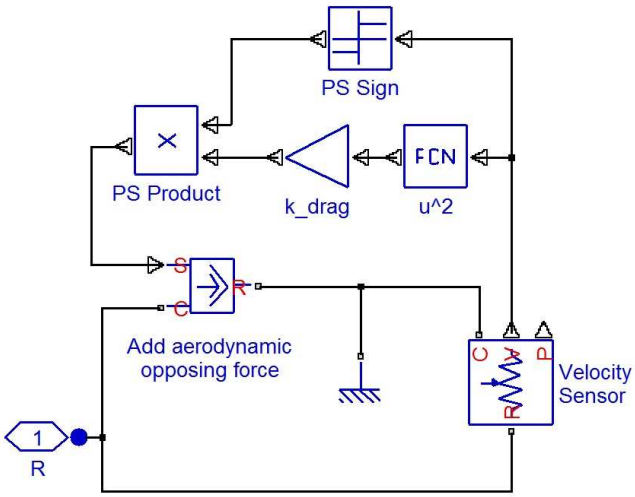

Figure 3.3: Aerodynamic Drag Simulink Model created by Simscape/Mechanical Library

In figure 3.3 k_drag is standing for $\frac{1}{2}\rho C_d A_f$. Left bottom of the figure 3.3, 'R', shows that aerodynamic drag model is directly added to the vehicle model.

3.1.4 Acceleration Force

In order to provide the required velocity change, an acceleration force should be given to the vehicle. This equation is the Newton's second law as in the following:

$$F_a = M_{eff} \cdot a \tag{3}$$

where M_{eff} (kg) is the effective mass of the vehicle which can be defined as

$$M_{eff} = m + \frac{J_{rear\_wheel}}{r_{rear}^2} + \frac{J_{front\_wheel}}{r_{front}^2} \tag{4}$$

where J_{rear_wheel} and J_{front_wheel} (kgm^2) are the rear and front wheel inertia, r_{rear} and r_{front} (m) are the rear and front wheel radii.

3.1.5 Climbing Resistance Force

In the existence of a up-hill terrain, vehicle needs to overcome the climbing resistance force to due to the weight component along the slope. On the opposite side, in the existence of a down-hill, this climbing resistance force contributes to the tractive force. The climbing resistance force can be described as in the

following

$$F_c = m \cdot g \cdot \sin(\alpha) \tag{5}$$

where m (kg) is the mass of the vehicle, g (m/s^2) the gravitational constant, and α (rad) is the road angle.

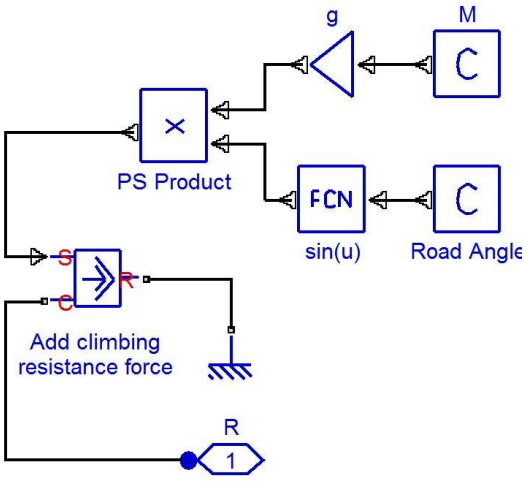

Figure 3.4: Climbing Resistance Model created by Simscape/Mechanical Library

3.1.6 Total Tractive Force

Total tractive force is the sum of the forces defined in 1, 2, 3 and 6.

$$F_{traction} = F_r + F_{aero} + F_a + F_c \tag{6}$$

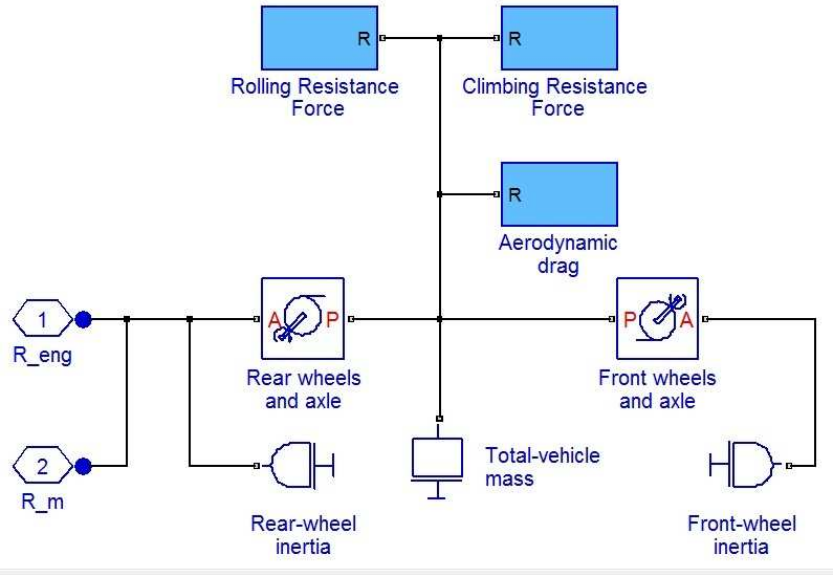

Figure 3.5: Karting Vehicle Simulink Model created by Simscape/Mechanical Library

3.2 Driving Cycles

Driving cycles are formulated in a way to measure the pollutant emissions and fuel consumptions. They are also used to formulate the vehicle emission regulations as well as to develop a car model. Therefore, for different driving ranges and conditions, various driving cycles are developed. Most cities have different traffic capacities and road conditions. Therefore, optimization of a driving cycle for a specific city condition will be better for testing.

3.2.1 ECE15

ECE Urban Driving Cycle has been using with EUDC (Extra Urban Driving Cycle) to test the emission and for certification in Europe. Since EUDC includes 120 km/h, it would not be possible to test it with a karting vehicle as in this study. Therefore, ECE cycle is used for the simulations and tests.

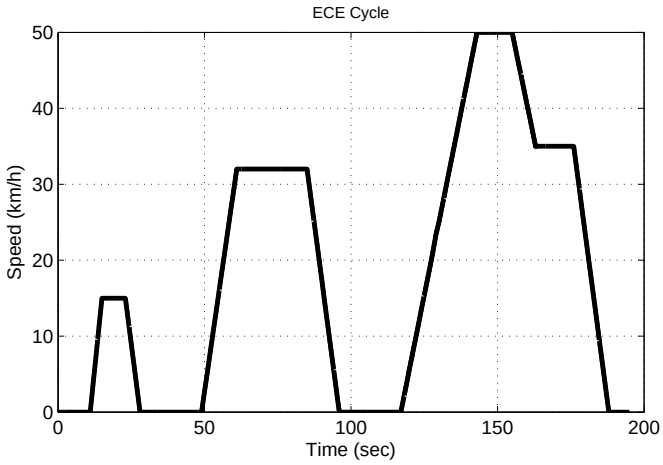

Figure 3.6: ECE cycle

3.3 Battery Model

In this work, it is intended to calculate, measure, and compare the performances of ultracapacitor module and lead acid battery groups. In battery modeling, battery SOC, temperature and

charging and discharging resistances are simulated.

3.3.1 Super-Capacitor Model

Open circuit ultracapacitor voltage

$$V_{OC} = SOC(V_{max} - V_{min}) + V_{min} \tag{7}$$

where $V_{max} = 2.7V$ and $V_{min} = 0$.

3.3.1.1 State of Charge Calculation

$$V_{OC}(n+1) = V_{OC}(n) - I\frac{dt}{C_{module}} \tag{8}$$

$$SOC = \frac{V_{OC}(n+1) - V_{min}}{V_{max} - V_{min}} \tag{9}$$

Here, capacitance 'C' can be found by interpolation for given current and temperature values. Changing capacitance value of the ultracapacitor cells with respect to output current and temperature values can be observed in figure 3.7

Total capacitance value of the ultracapacitor module can be found by the following equation

$$C_{module} = C_{cell}/\#\_of\_cell \tag{10}$$

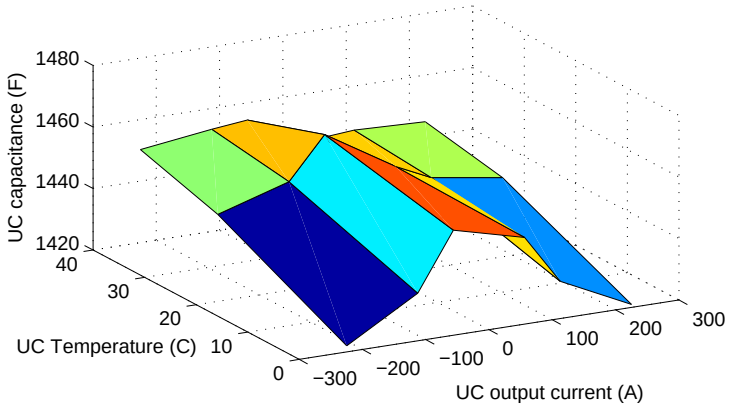

Figure 3.7: Ultracapacitor cell capacitance with respect to changing current and temperature values

3.3.1.2 Output Current Calculation

$$I_{out} = \frac{V_{OC} - (V_{OC}^2 - 4RP_{out})^5}{2R} \tag{11}$$

where R is the resistance of the ultracapacitor. It changes in charging and discharging processes. While the ultracapacitor resistance shows differences with the changing temperature and current. Instantaneous resistance of ultracapacitor can be found from the figure 3.8 for given temperature and current values.

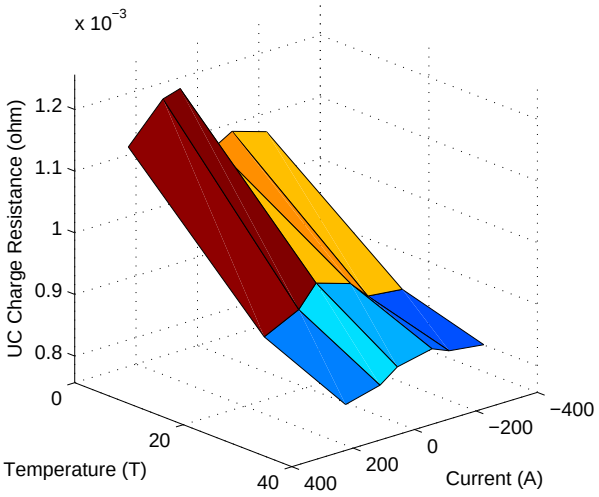

Figure 3.8: Ultracapacitor cell resistance with respect to changing current and temperature values

The total ultracapacitor module resistance can be calculated as follows:

$$T = (\#\_of\_cell) \cdot R_{cell} \tag{12}$$

The resistance calculation illustration can be found in figure 3.9.

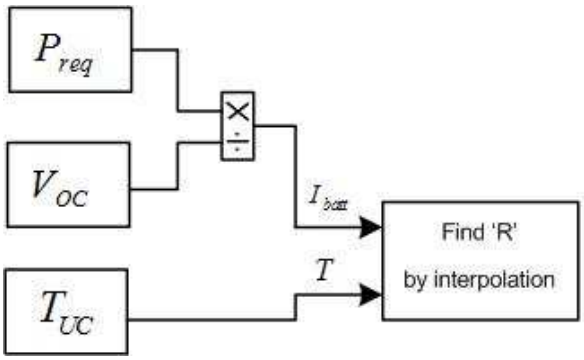

Figure 3.9: Resistance find by interpolation in look-up table whose elements are given current and temperature data

In the model it is checked that charging current does not exceed the charging limit and maximum current is enforced. Moreover, decharging current is also checked with the minimum decharging current. In the case of low currents battery current is kept at or above the minimum. Maximum charging and minimum decharging currents can be found as in the following

$$I_{chg\_max} = \frac{V_{OC} - V_{max}}{R} \tag{13}$$

$$I_{dischg\_min} = \frac{V_{OC} - V_{max}}{R} \tag{14}$$

3.3.1.3 Output Voltage Calculation

Ultracapacitor output voltage can be found as in the following

$$V_{out} = V_{OC} - \frac{I_{out}}{R} \tag{15}$$

3.3.2 Lead Acid Battery Model

In the simulation environment, the model developed by [47] is used for lead acid batteries. The model has been applied for 56Ah 12V car battery. The equivalent circuit of the model is shown in figure 3.10.

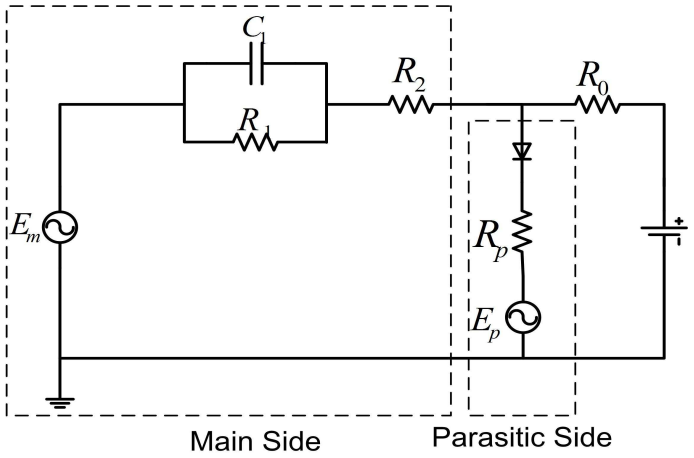

Figure 3.10: Equivalent Circuit of Lead Acid Battery

The set of equations for the model described in figure 3.10 is provided below as

- Main Branch Voltage

$$V_{main} = V_{main\_0} - K_E(273 + T)(1 - SOC) \qquad (16)$$

where V_{main} (V) is the main branch open circuit voltage, V_{main_0} (V) is the main branch open circuit voltage at full charge and K_e $(V/^\circ C)$ is a constant.

- Terminal Resistance

$$R_0 = R_{0\_initial}[1 + \zeta_0(1 - SOC)] \qquad (17)$$

where R_0 (ohm) is the terminal resistance, $R_{0\_initial}$ (ohm) is the resistance value when SOC is 1 and ζ_0 is a constant.

- Main Branch Resistance 1

$$R_1 = -R_{1\_initial} ln(DOC) \qquad (18)$$

where R_1 (ohm) is the main branch resistance, $R_{1\_initial}$ (ohm) is the resistance value when SOC is 1.

- Main Branch Capacitance

$$C_1 = \tau_1 / R_1 \qquad (19)$$

where C_1 (F) is the main branch capacitance, τ_1 is the main branch time constant.

- Main Branch Resistance 2

$$R_2 = R_{2\_initial} \frac{e^{[\zeta_1(1-SOC)]}}{1 + e^{[\zeta_2(I_{main}/I*)]}} \tag{20}$$

R_2 (ohm) is main branch resistance, $R_{2\_initial}$ is a constant, ζ_1 and ζ_2 are constant. I_{main} is the main branch resistance and $I*$ (A) is the nominal battery current.

- Parasitic Branch Current

$$I_p = V_p G_p e^{(\frac{V_p/(\tau_p s+1)}{V_{p\_0}} + \zeta_3(1-\frac{T}{T_f}))} \tag{21}$$

where I_p (A) is the current loss at parasitic branch, V_p is the voltage at parasitic branch, τ_p (s) parasitic branch time constant, V_{p_0} (V) , G_p (s) and ζ_3 are constant, T_f $(^\circ C)$ is the freezing temperature of the electrolyte.

- Extracted Charge

$$Q_e(t) = Q_{e_init} + \int_0^t -I_m(\tau)d\tau \tag{22}$$

where Q_e $(Amp - sec)$ is the extracted charge and Q_{e_init}

$(Amp - sec)$ is the initial extracted charge and I_m (A) id the main branch current.

- Total Capacity

$$C(I, Q) = \frac{K_c C_o K_t}{1 + (K_c - 1)(I/I*)^{\delta}} \tag{23}$$

where K_c and δ are constant, C_0 $(Amp - sec)$ is no load capacity, and K_t is temperature dependent constant.

- State of Charge and Depth of Charge

$$SOC = 1 - \frac{Q_e}{C(0, Q)} \tag{24}$$

$$DOC = 1 - \frac{Q_e}{C(I_{avg}, Q)} \tag{25}$$

- Estimate of Average Current

$$I_{avg} = \frac{I_m}{\tau_1 s + 1} \tag{26}$$

where I_avg (A) is the main branch average current and τ_1 (sec) is the main branch time constant

Integration of electric motor with lead acid battery group in the simulation environment, can be found in figure 3.11.

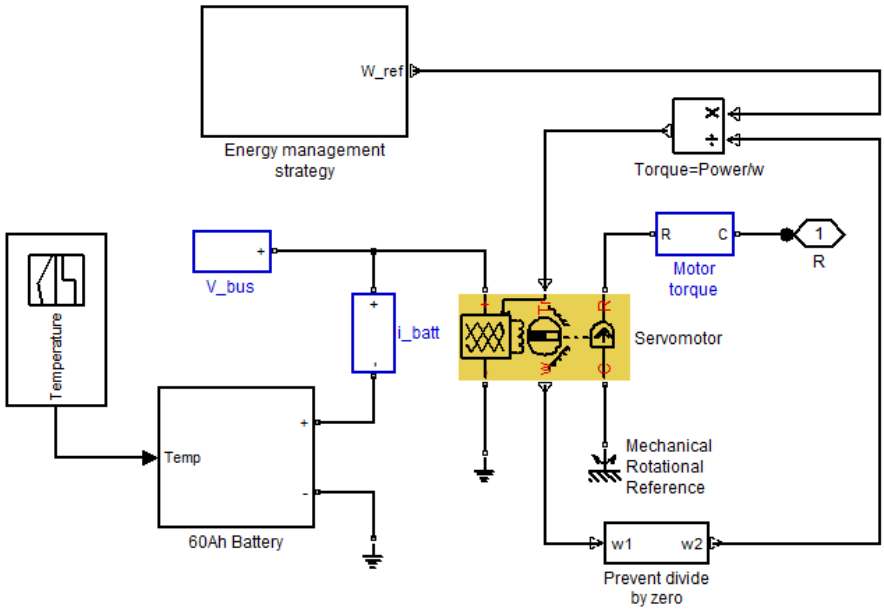

Figure 3.11: Lead Acid Battery group, electric motor and shaft integration in Matlab/Simulink.

3.4 Parallel Hybrid Karting Vehicle Control

In this work, hybrid karting vehicle traction power is shared between electric motor and the internal combustion engine. The electric motor boosts the ICE power. The electrical motor is controlled according to vehicle power demand condition. Since the total traction power is shared between the electric motor and the ICE, the electric motor provides complementary power to the traction effort. In the simulation environment, driver's

input torque is modeled in a way that, for given a driving cycle speed profile can be tracked

3.4.1 Driver's Input Torque Model

In this work, driver would like to track the velocity trajectory which is specified before. In the simulation environment, driver's force demand is calculated with an integration of controller to the vehicle's tractive force model. The tractive force is mainly described as follows

$$F_{traction} = F_r + F_{aero} + F_a + F_c \tag{27}$$

Traction power is calculated as

$$T_{traction} = (F_r + F_{aero} + F_a + F_c) \cdot r_{rear\_wheel} \tag{28}$$

Since the electric motor is directly attached to the vehicle shaft, electric motor will be directly affecting the driving performance as well. In terms of engine and motor torques traction power can be described as

$$T_{traction} = T_m + T_{eng} \tag{29}$$

Based on the equations 28 and 29, the engine torque model can be described as

$$T_{eng} = (F_r + F_{aero} + F_a + F_c) \cdot r_{rear\_wheel} - T_m \tag{30}$$

However, in our developed karting model, there is no feedback information about how much the electrical motor is assisting to system. Driver also needs to compensate the power added to the system by the electric motor in order to follow the desired velocity trajectory. Therefore, in the simulation environment motor torque is compensated with a sliding mode controller.

$$T_{eng} = (F_r + F_{aero} + F_a + F_c) \cdot r_{rear\_wheel} - f_v s - \kappa sat(s) \tag{31}$$

where f_v is for transient duration adjustment, $sat(s)$ is saturation function which is defined in equation 78. s is the sliding surface which is defined as in the following:

$$s = e + \Lambda \dot{e} \tag{32}$$

where $e = q - q_{ref}$ and $\dot{e} = w - w_{ref}$.

$$sat(s) = \begin{cases} 1 & s > \epsilon \\ s/\epsilon & |s| \leq \epsilon \\ -1 & s < -\epsilon \end{cases} \tag{33}$$

Lyapunov function candidate is selected as

$$V(s) = \frac{1}{2} s^T M_{eff} s \tag{34}$$

Differentiating V(s) with respect to time, using the model equation, one can obtain the following

$$\dot{V} = -s^T \Lambda [f_v s + K sat(s) - T_m] \tag{35}$$

Define T_v as error due to parameter estimation with bounded motor torque

$$\|T_m\| \leq \nu \|s\| \tag{36}$$

with a certain bound ν, $K \geq \nu$

$$\dot{V}(s) \leq -s^T f_v \Lambda s - (K - \nu)\Lambda \|s\| \leq 0 \tag{37}$$

Now, one can evaluate the stability of the system.

In order to increase the fuel economy of the vehicle, energy

management strategy should be selected such that engine works at its efficient regions. This way, engine losses will be diminished and fuel economy will be improved. The control strategy should be managed carefully in order not to deteriorate the performance.

3.4.2 Electrical Motor Control Strategies

Electrical motor control has been studied by finite state machine control strategy, charge sustaining control strategy, and optimal control strategy separately. Finite state machine control is a rule based control strategy which depends on limited rules. In the charge sustaining control strategy, it is aimed to keep the SOC level in the given interval. Moreover, by the optimal control strategy, an optimum electrical motor performance is modeled in a way that fuel minimization is realized while the constraint of SOC is kept at specified rate at the end of the driving range. These three control strategies are developed and implemented in order to evaluate their performances, and to find the suitable control strategy on a given driving range for the hybrid vehicle.

3.4.2.1 Finite State Machine Control Strategy

In the start-up and acceleration time interval of the vehicle, engine burns extra fuel. In this control strategy, it is aimed that electric motor to assist in the vehicle start-up/acceleration process where the engine is running in inefficient region. The electric motor also assists during vehicle speed up and passing conditions. During cruising time intervals, electric motor aids the traction effort. In the deceleration time intervals, motor functions as generator to convert the kinetic energy of the vehicle into electrical energy. This way, regenerative brake energy will be stored in batteries for the following start-up/acceleration time interval.

In finite state machine control strategy, battery state of charge condition is also important. SOC working range is chosen as %50 - %100, when the battery charge level drops below %50, electrical motor cannot assist the traction effort until the next deceleration time interval when the batteries can be charged again. The rules can be modified in a way such that batteries can be charged during cruising time intervals where the traction effort is not much.

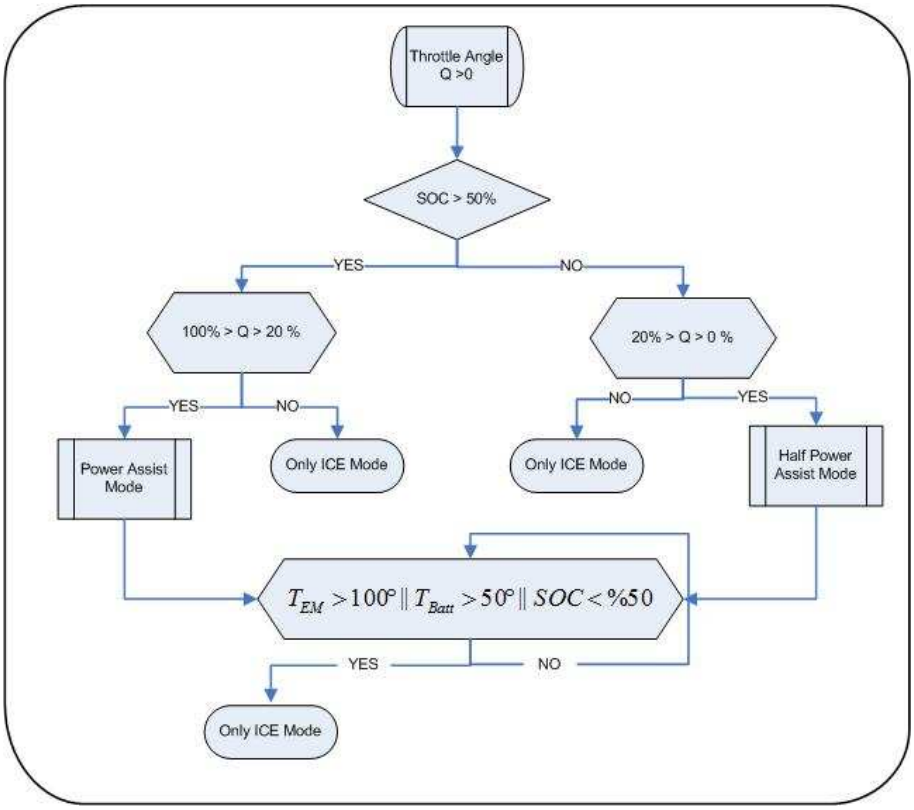

Figure 3.12: Starting and passing decision algorithm

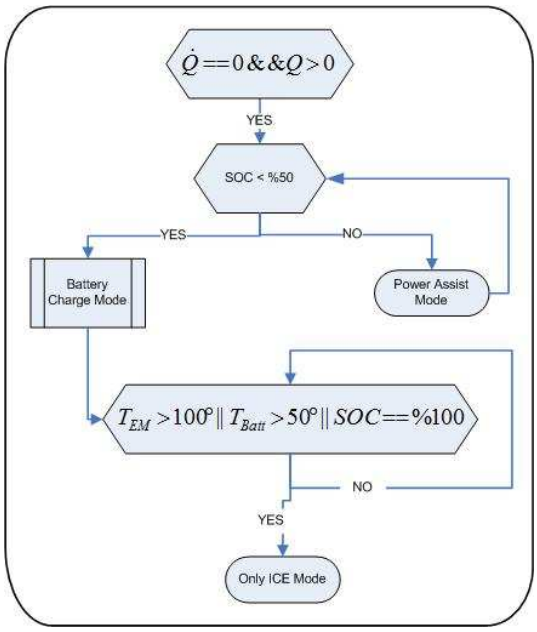

Figure 3.13: Cruising decision algorithm

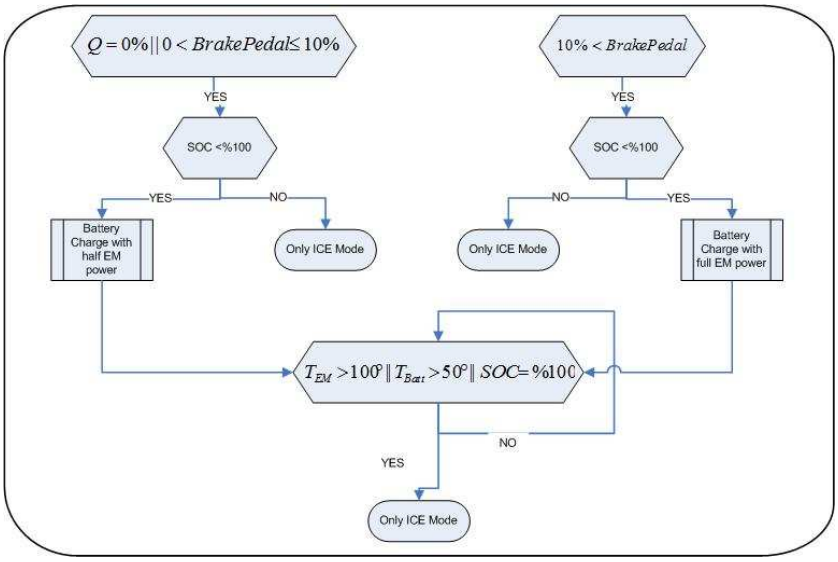

Figure 3.14: Charging decision algorithm

3.4.2.2 Charge Sustaining Control Strategy

Optimum control may give the best efficiency among the other control strategies. However, road and battery conditions cannot be predicted during an actual driving range. Therefore, a control algorithm which sustains the system would be preferable. The idea of the charge sustaining control strategy is based on keeping the charge level of the battery in a desired range. According to throttle demand and state of charge level, motor effort can be calculated so that batteries can be filled if the SOC level is low, and traction effort can be aided by electric motor if the SOC level is high enough. Electric motor control effort and ICE engine required power levels are formulated with the knowledge of SOC level and throttle angle.

The total power that is supplied by engine and electric motor can be defined as follow

$$P_m + P_{eng} = P_{total} \tag{38}$$

Since they drive the same shaft, the rotational speed is equal on both of engine and electrical motor. Therefore, we can describe the equation (38) as

$$(T_m + T_{eng}) \cdot w = T_{total} \cdot w \tag{39}$$

Simulation of vehicle engine torque vs rotational speed is provided with a graph in figure 3.15.

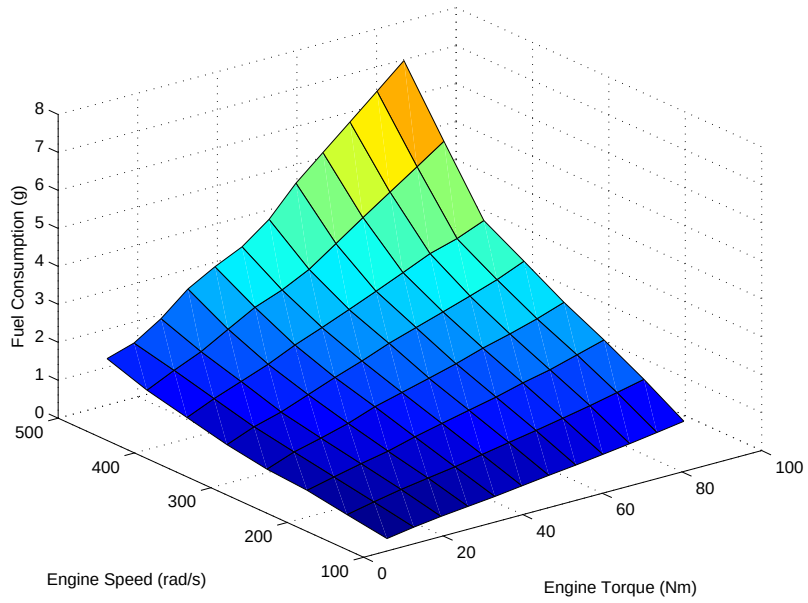

Figure 3.15: Fuel consumption graph for given engine torque and angular velocity

In order to reduce the fuel consumption, at a given speed engine

$$\overline{SOC} = \frac{SOC_{high} + SOC_{low}}{2} \tag{40}$$

$$\Delta SOC = \overline{SOC} - SOC \tag{41}$$

Normalized SOC can be defined as in the equation (42)

$$N = \frac{-2 \cdot \Delta SOC}{SOC_{high}} \tag{42}$$

Saturation point for charging is defined with the parameter S_c. The saturation point for discharging is defined with the parameter S_d. Moreover, throttle range for charge and discharge conditions are defined with the parameters and Q_{th-ch} and $Q_{th-disch}$. These can calculated with the given formulas (43) and (44)

$$Q_{th-ch} = Q_{up} - Q \tag{43}$$

$$Q_{th-disch} = Q - Q_{low} \tag{44}$$

where Q_{low} and Q_{up} are the lower and the upper limit of the throttle.

The needed throttle deviation from the nominal throttle angle, in order to sustain the charging discharging balance in the starting, cruising and decelerating processes, can be described

as in the following.

- When $N < -1$

$$\Delta Q = \begin{cases} Q_{th-ch} \cdot (-N) & \text{if } S_c \leq N \\ Q_{th-ch} & \text{if } N < S_c \end{cases} \tag{45}$$

- When $N \geq -1$

$$\Delta Q = \begin{cases} -Q_{th-disch} \cdot (N) & \text{if } S_d \leq N; \\ -Q_{th-disch} & \text{if } N < S_p; \end{cases} \tag{46}$$

During idle condition of the vehicle the needed throttle position, to sustain the charge balance is described as in the following

- When $N < 0$

$$\Delta Q = \begin{cases} Q_{base} + \lambda \cdot Q_{th-ch} \cdot (-N) & \text{if } S_c \leq N \\ Q_{base} + \lambda \cdot Q_{th-ch} & \text{if } N < S_c \end{cases} \tag{47}$$

- When $N \geq 0$

$$\Delta Q = \begin{cases} Q_{base} + \lambda \cdot Q_{th-ch} \cdot (-N) & \text{if } S_c \leq N \\ Q_{base} + \lambda \cdot Q_{th-ch} & \text{if } N < S_c \end{cases} \tag{48}$$

Now, total torque on vehicle shaft can be described as in the following

- When $V_{vehicle} > 0$ (accelerating, cruising and decelerating processes)

$$T_{total} = \underbrace{(\gamma_1(w) \cdot \Delta Q + T_{traction})}_{T_{eng}} + \underbrace{\gamma_2(w) \cdot \Delta I_m}_{T_m} \tag{49}$$

- When $V_{vehicle} == 0$ (idle times)

$$T_{total} = \underbrace{(\gamma_3(w) \cdot Q)}_{T_{eng}} + \underbrace{\gamma_4(w) \cdot I_m}_{T_m} \tag{50}$$

3.4.2.3 Optimal Control Strategy

Optimal control strategies for hybrid vehicles can be grouped in two categories which are real time optimal control strategy and offline global optimization. Offline global optimization has been applied on given a driving cycle. Offline global optimization technic requires parameter tuning and computational time effort before implementation on a case. In this section, the optimization has been conducted on given driving cycle ECE which will be offline global optimization.

First of all, battery is modeled as a dynamical system with

x_b

$$x_b(t+1) = x_b(t) + P(T_m(t), w(t)) \cdot \Delta \tag{51}$$

where $P(T_m(t), w_m(t))$ represents the power required to produce torque T_m at a given speed w.

Energy required by the engine over an interval can be defined as

$$J = \int_{t=t_i}^{t=t_f} \dot{m}(T_m(t), w(t))\mathrm{d}t \tag{52}$$

Fuel consumption can also be described over N samples as in the following

$$J = \sum_{t=0}^{N-1} \dot{m}(T_m(t), w(t)) \cdot \Delta \tag{53}$$

Mechanical constraints can be defined as in the following.

- Rotational speed constraint

$$w_{min} < w(t) < w_{max} \tag{54}$$

- Torque constraint

$$0 \leq T_m(t) \leq T_m(w(t)) \tag{55}$$

Maximum motor torque with respect to changing motor speed can be found in figure 3.16.

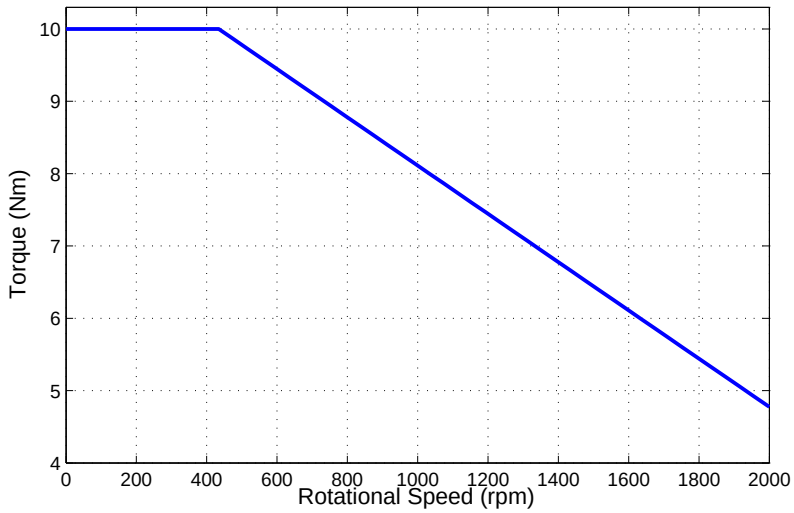

Figure 3.16: Motor torque graphic with respect to motor speed

Torque relation between motor and engine as in the following

$$T_m + T_{eng} = T_{traction} \tag{56}$$

Problem Formulation In the optimal control problem, fuel consumption will be minimized over a period

$$\min_{T_m(t), w(t)} J = \sum_{t=0}^{N-1} F(T_m(t), w(t)) \cdot \Delta \tag{57}$$

Mechanical constraint torque will have role on optimization problem

$$0 \leq T_m(t) \leq T_m(w(t)) \tag{58}$$

Over one period of the driving cycle, state of the battery charge is kept constant. In addition to the constraint defined in formula (59), the following constraint is also defined.

$$x(N) - x(0) = 0 \tag{59}$$

This constraint is used to keep the state of charge for battery constant at the initial state. This way, the battery is in ready condition for the next period. In this optimum control problem, periods are defined as:

'At the beginning of the period, initial velocity is zero and at the end of the period final velocity is zero. Each period cycle has acceleration and deceleration time intervals.'

Motor torque constraint inequality can be converted into equality with a new variable κ.

$$T_m(t)^2 + \gamma_1(w(t), t) \cdot T_m + \gamma_2(w(t), t) + \kappa^2 = 0 \tag{60}$$

Now, overall problem definition can be defined as in the following

$$\begin{aligned}\min_{T_m(t),w(t)} J = \sum_{t=0}^{N-1} (&F(T_m(t), w(t)) \cdot \Delta \\ &+ \lambda_1(t) \cdot (x_b(t+1) - x_b(t) - P(T_m(t), w(t)) \cdot \Delta) \\ &+ \lambda_2(t) \cdot (T_m(t)^2 + \gamma_1(w(t), t) \cdot T_m + \gamma_2(w(t), t) + \kappa(t)^2))\end{aligned} \tag{61}$$

For the optimality condition, the followings should be satisfied

$$\frac{\partial J}{x_b(t)} = 0 \tag{62}$$

$$\frac{\partial J}{\lambda_1(t)} = 0 \tag{63}$$

$$\frac{\partial J}{\lambda_2(t)} = 0 \tag{64}$$

$$\frac{\partial J}{T_m(t)} = 0 \tag{65}$$

$$\frac{\partial J}{\kappa(t)} = 0 \tag{66}$$

According to the equation (62), $\lambda_1(t) = \lambda_1(t+1)$ should be satisfied for each sampling time. Moreover, (66) results with

$$2 \cdot \lambda_2(t) \cdot \kappa(t) = 0 \tag{67}$$

With the choice of $\lambda_2(t) = 0$, equation (61) simplifies to

$$\begin{aligned} \min_{T_m(t),w(t)} J = \sum_{t=0}^{N-1} (& F(T_m(t), w(t)) \cdot \Delta \\ & + \lambda_1(t) \cdot (x_b(t+1) - x_b(t) - P(T_m(t), w(t)) \cdot \Delta)) \end{aligned} \tag{68}$$

Applying the condition given in equation (59) on equation (68) and considering the equality $\lambda_1(t) = \lambda_1(t+1)$, equation (68) becomes

$$\min_{T_m(t),w(t)} J = \sum_{t=0}^{N-1} (F(T_m(t), w(t)) \cdot \Delta$$

,

$$+ \lambda_1 \cdot (-P(T_m(t), w(t)) \cdot \Delta)) + \lambda_1 (x_b(t+1) - x_b(t)) \tag{69}$$

Control input can be finalized with the following

$$\min_{T_m(t),w(t)} J = \sum_{t=0}^{N-1} (F(T_m(t), w(t)) \cdot \Delta + \lambda_1 \cdot (-P(T_m(t), w(t)) \cdot \Delta)) \tag{70}$$

By the choice of λ_1, T_m will be determined for each sampling time. Results and discussion regarding this issue can be found in chapter 4.

3.4.3 DC PM Motor Control Strategy for Experiments

The torque obtained with the control strategies described at section 3.4.2 are applied on the DC PM motor during the experiment. Obtained torque reference is applied to the test bench motor with the sliding mode controller which is described in the following.

Torque equality can be described as

$$T_{ref} = T_i + T_\mu + T_f(q, w) \tag{71}$$

$$T_\mu = \mu w \tag{72}$$

where the w (rpm) represents the angular velocity and μ (Nm/rpm) represents the viscous friction coefficient.

$$T_i = J\dot{w} \tag{73}$$

Reference torque 74 is the product of motor torque constant k_t and reference current, which overcomes the torque due to stiction, viscosity and inertia.

$$T_{ref} = k_t i_{ref} \tag{74}$$

$$k_t i = J\dot{w} + \mu w + T_f(q, w) \tag{75}$$

Reference current is chosen as in the following

$$k_{t_0} i = J_o \dot{w} + \mu_0 w - f_v s - \kappa sat(s) \tag{76}$$

where f_v is for transient duration adjustment, $sat(s)$ is sat-

uration function which is defined in equation 78 and s is the sliding surface which is defined as in the following.

$$s = e + \Lambda \dot{e} \tag{77}$$

where $e = q - q_{ref}$ and $\dot{e} = w - w_{ref}$.

$$sat(s) = \begin{cases} 1 & s > \epsilon \\ s/\epsilon & |s| \leq \epsilon \\ -1 & s < -\epsilon \end{cases} \tag{78}$$

Lyapunov function candidate is chosen as

$$V(s) = \frac{1}{2} s^T J s \tag{79}$$

Differentiating V(s) with respect to time, using the model equation, one can obtain the following

$$\dot{V} = -s^T \Lambda [f_v s + K sat(s) - T_v(i, w)] \tag{80}$$

Defining T_v which is errors due to parameter estimation errors

$$T_v(i, w) = J[J^{-1}(k_t i - \mu w - T_f) - J_0^{-1}(k_{t_0} i - \mu_o w - T_{f_0})] \tag{81}$$

with the bounded parameter estimation error

$$\|T_v(i,w)\| \leq \nu\|s\| \tag{82}$$

with a certain bound ν, $K \geq \nu$

$$\dot{V}(s) \leq -s^T f_v \Lambda s - (K-\nu)\Lambda\|s\| \leq 0 \tag{83}$$

Now, one can evaluate the stability of the system.

Chapter IV

4 Simulation Results and Discussion

Simulations have been performed with the model described in chapter 3. Simulation parameters can be found in table 4.1. Here, "m" stands for the overall mass of the karting vehicle with its driver, electric motor and batteries.

System Parameters	**Values**
m	$180kg$
r_{rear}	$0.1m$
r_{front}	$0.07m$
J_{front_wheel}	$0.05kgm^2$
J_{rear_wheel}	$0.06kgm^2$
ρ	$1.2kg/m^3$
C_d	0.5
A_f	$1m^2$

Table 4.1: Simulation Parameters of Karting Vehicle

4.1 Rule-Based Control Strategy Simulation Results

Hybrid karting vehicle's electric motor has been controlled with the rules specified in figures 3.12, 3.13 and 3.14. Driver follows the trajectory given by ECE15. Driver input torque is calculated as described in the section 3.4.1 with sliding mode controller. In real case, driver input torque would be managed by the ICE through the throttle and brake pedals.

As it can be seen in figures 4.1 and 4.5, during acceleration time intervals the current sign is negative which means charge is depleting. During deceleration time intervals, the current sign becomes positive which means batteries are charging with the regenerative brake energy. Correspondingly, battery voltages and SOC levels are decreasing while battery charge is depleting, and increasing while battery is charging.

4.1.1 Results with Ultracapacitor

During simulations and tests with ultracapacitor system, a module whith 83F and 48V has been selected as the storage package. The reference speed given as in figure 4.4 with the control of engine torque. Electric motor aides with the traction torque which is controlled by a rule based controller. The

obtained motor torque can be seen in figure 4.1. During speed-up/acceleration processes of the vehicle, electric motor generates positive torque. During deceleration time intervals, it functions as a generator, and its torque is negative to help the vehicle to slow down.

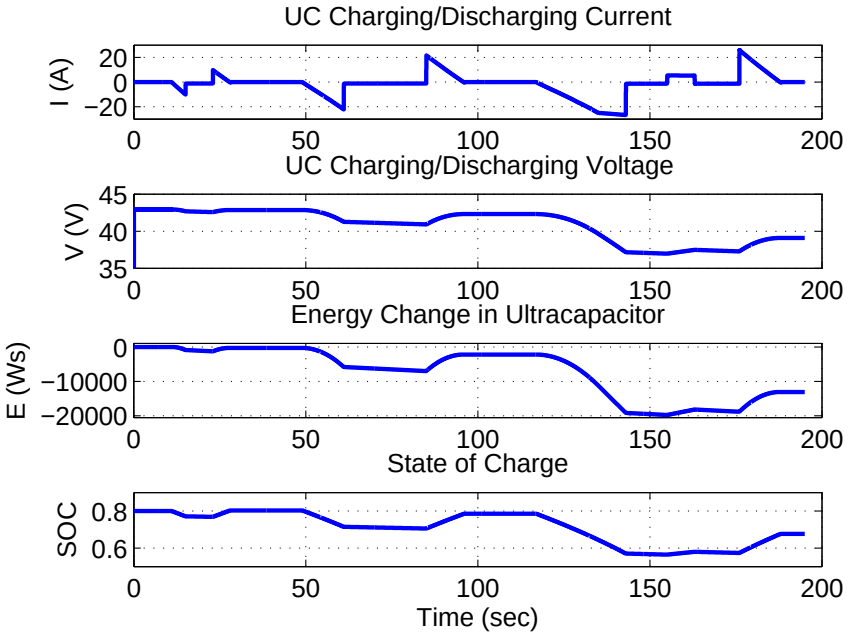

Figure 4.1: Lead acid battery current, voltage, energy and state of charge variations by time with the UC usage in the Rule Based control strategy

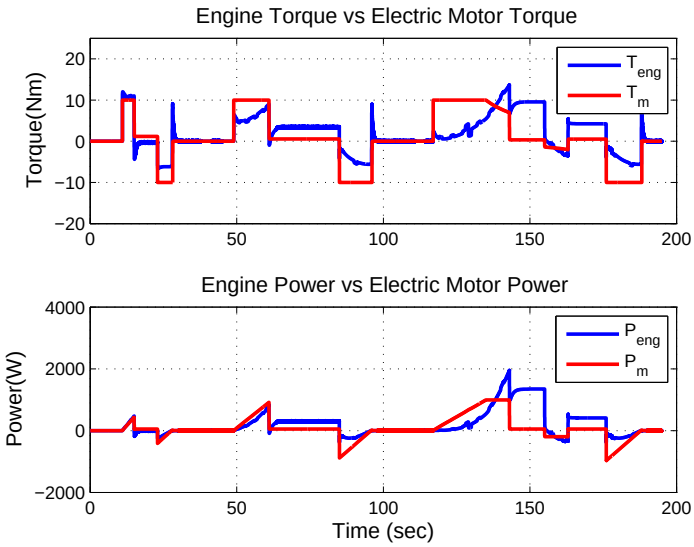

Figure 4.2: Motor and engine torque and power variations by time with the UC usage in the Rule Based control strategy

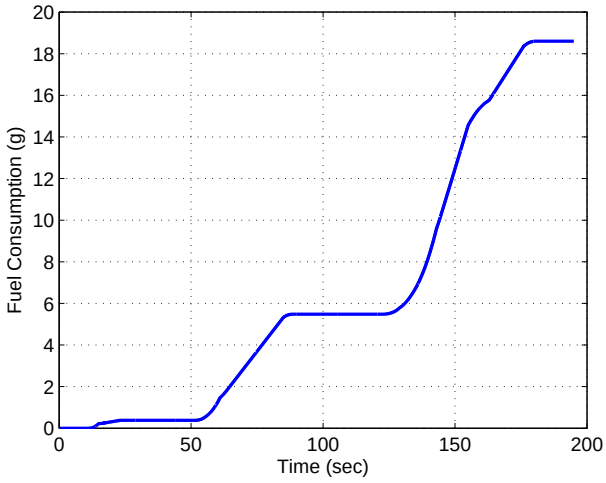

Figure 4.3: Total fuel consumption by time with the UC usage in the Rule Based control strategy

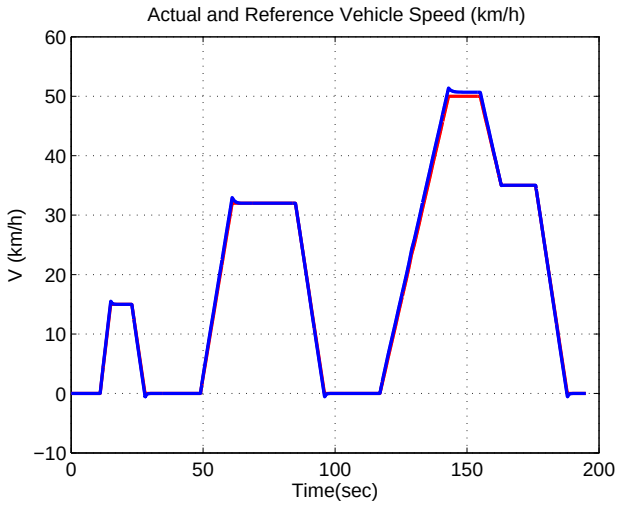

Figure 4.4: Actual and Reference Vehicle Speed with the UC usage in the Rule Based control strategy

4.1.2 Results with Lead Acid Battery

In these simulations, lead acid car batteries with 12V and 60Ah have been used. Two of them were connected in series as a battery package. While the vehicle is tracking the reference speed given in figure 4.8 with the control of engine torque, motor aids the traction torque which is controlled by a rule based controller. The obtained motor torque can be seen in figure 4.6. During the speed-up/acceleration processes of the vehicle, electric motor generates positive torque. During the deceleration time intervals it functions as a generator.

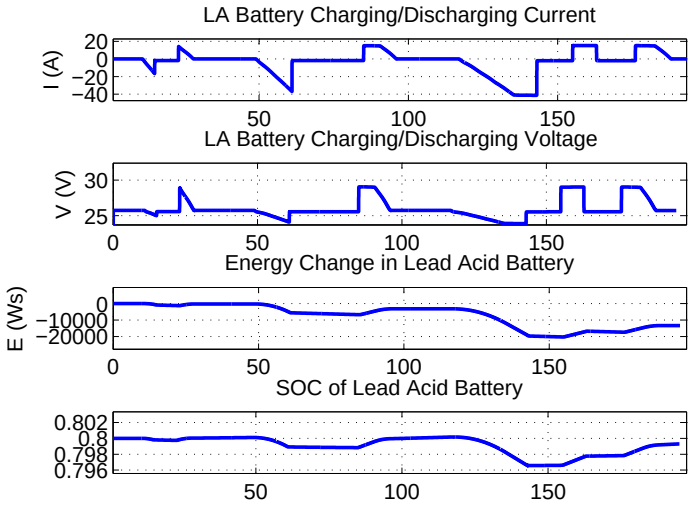

Figure 4.5: Lead acid battery current, voltage, energy and state of charge variations by time with the LA usage in the Rule Based control strategy

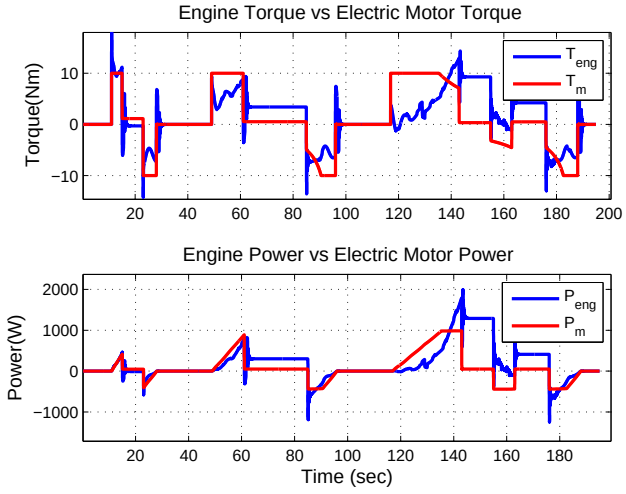

Figure 4.6: Motor and engine torque and power variations by time with the LA usage in the Rule Based control strategy

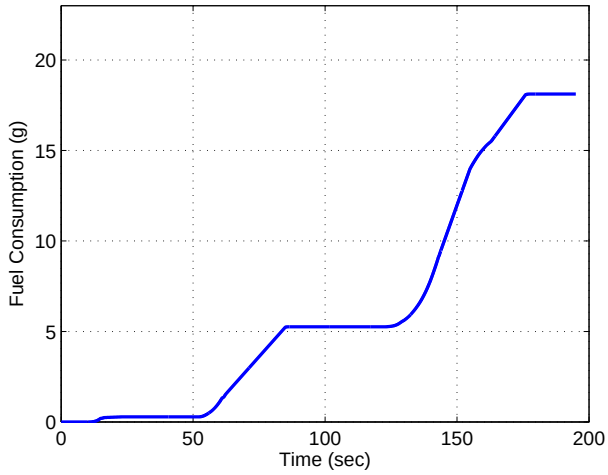

Figure 4.7: Total fuel consumption by time with the LA usage in the Charge Sustaining control strategy

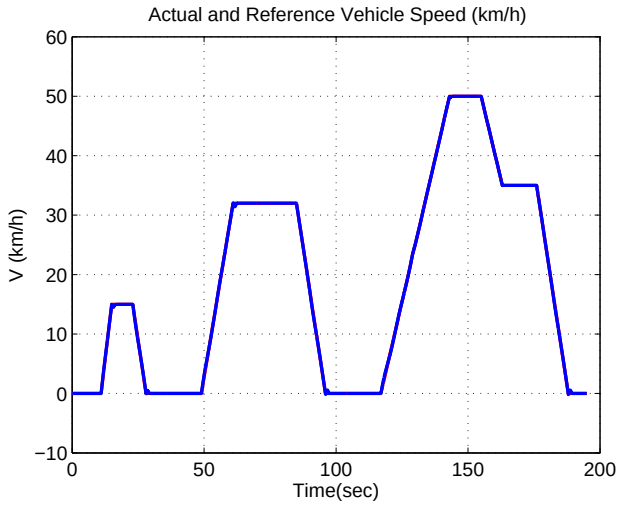

Figure 4.8: Actual and Reference Vehicle Speed with the LA usage in the Rule Based control strategy

While the vehicle's internal combustion engine consumes 44.7 kWs energy with the ultracapacitor battery pack, it consumes 46.32 kWs energy with the lead acid battery pack. In the time intervals of the electric motor assist, electric motor consumes 26.2 kWs with the ultracapacitor battery pack, it consumes 25.50 kWs energy with the lead acid battery pack. In the regenerative breaking time intervals, while ultracapacitor package saves 13.13 kWs energy, lead acid battery saves 11.8 kWs.

These results show that the usage of UC battery pack and LA battery pack does not make any significant difference. It only matters in terms of energy recuperation.

4.2 Charge Sustaining Control Strategy Simulation Results

Hybrid karting vehicle's electric motor has been directed with the control algorithm specified in section 3.4.2.2. Charge sustaining control strategy parameters can be found in table 4.2. Herein, ECE15 driving cycle is followed. Driver's input torque is calculated as described in the section 3.4.1 with a sliding mode controller.

As it can be seen in figures 4.10 and 4.16, during the accel-

eration time intervals current is negative which shows charge is depleting. During the deceleration time intervals, the current is positive which shows that batteries are charging with the regenerative brake energy. Correspondingly, battery voltages and SOC levels are decreasing while battery charge is depleting, and increasing while battery is charging.

Control Parameters	**Values**
λ	0.1
S_c	0.5
S_d	-0.5
Q_{up}	60
Q_{low}	0
Q_{base}	2

Table 4.2: Charge Sustaining Control Strategy Simulation Parameters and their values.

Scaling factor λ is used in order to adjust the energy conversion from electric motor to the supercapacitor/lead acid battery during idle time.

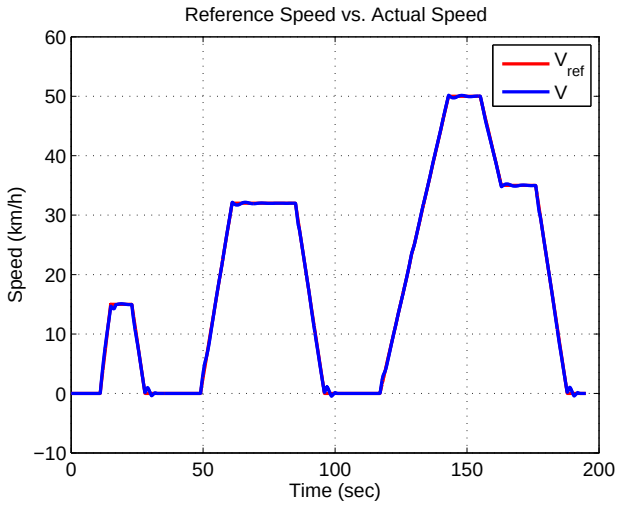

Figure 4.9: Reference speed and actual speed with Charge Sustaining Control

4.2.1 Results with Ultracapacitor (UC)

In this part of the work, a 83F and 48V ultracapacitor module has been used. The reference speed given in figure 4.25 with the control of engine torque. The motor aids the traction torque which is controlled by charge sustaining control algorithm. The resulting motor torque can be seen in figure 4.12. During the speed-up/acceleration processes of the vehicle, electric motor generates positive torque. During the deceleration time intervals it performs as a generator, and its torque is negative in these intervals which helps the vehicle to slow down.

While ultracapacitor's charge condition is %80 at the begin-

ning of the simulation, at the end its SOC has fallen to %70.04. In this control strategy, it is aimed to keep the battery SOC between %50-%100. So that, battery full depletion will not be realized during long driving cycles.

As it can be seen in figure 4.13, fuel consumption with charge sustaining control strategy is $18.73g$ with the use of ultracapacitor as the storage media.

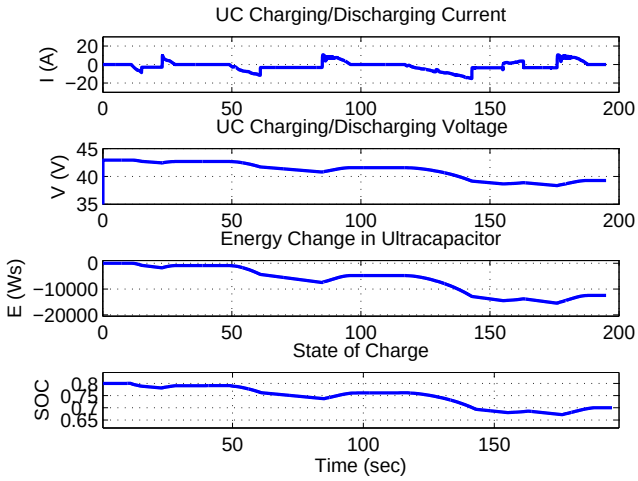

Figure 4.10: UC current, voltage, energy and state of charge variations with the UC usage in the Charge Sustaining Control strategy

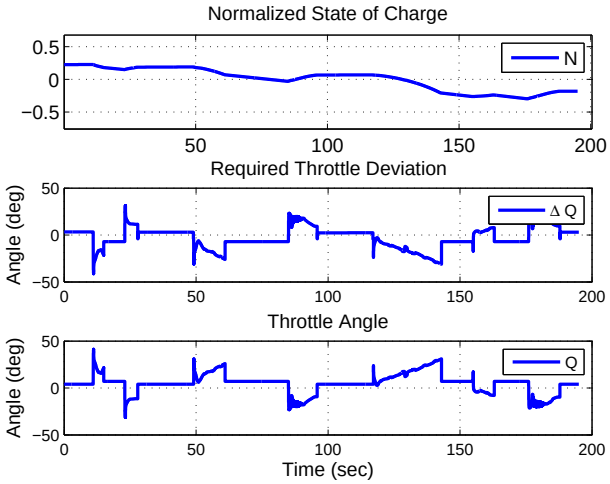

Figure 4.11: Normalized SOC, throttle angle deviation and throttle angle positions

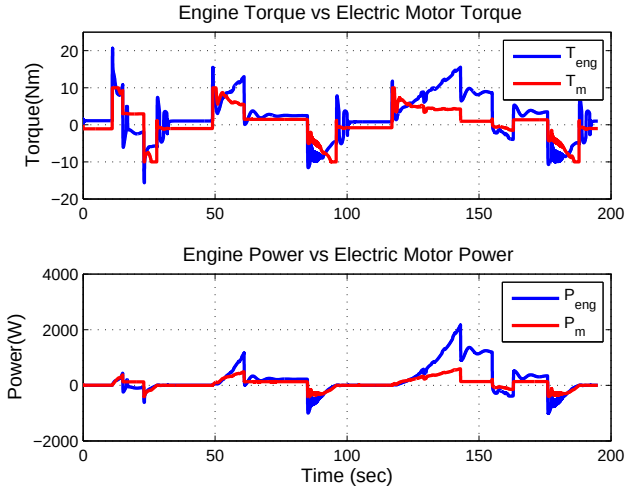

Figure 4.12: Motor and engine torque and power variations with the UC usage in the Charge Sustaining Control strategy

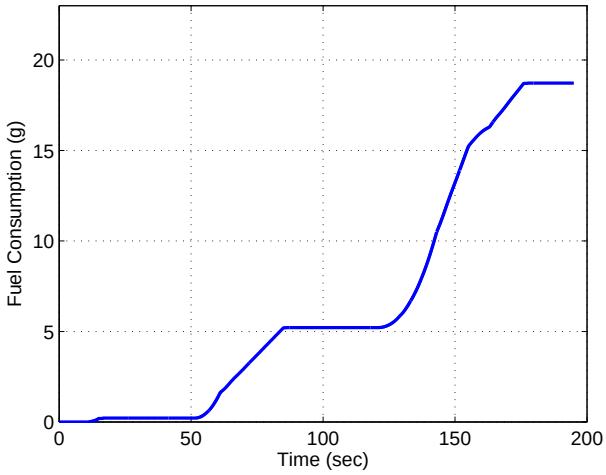

Figure 4.13: Total fuel consumption with the UC usage in the Charge Sustaining Control strategy

4.2.2 Results with Lead Acid Battery (LA)

In these simulations, lead acid car batteries have been used with 12V and 60Ah capacity. Two of them were connected in series as a battery package. The reference speed is given in figure 4.25 with the control of engine torque. The motor aids the traction torque which is controlled by charge sustaining controller. The obtained motor torque can be seen in figure 4.15. In the speed-up/acceleration processes of the vehicle, electric motor boosts the traction power, and in the deceleration time intervals it functions as a generator.

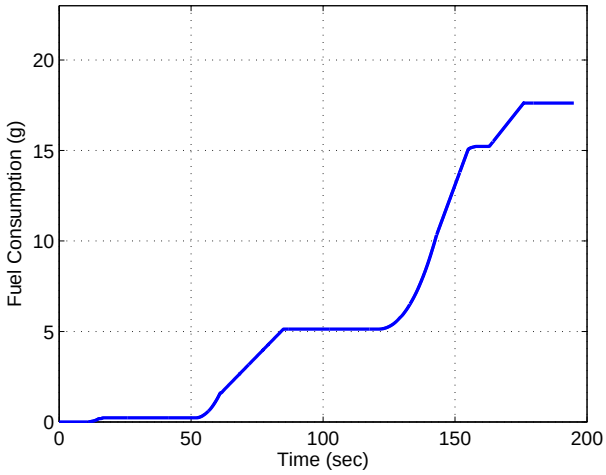

Figure 4.14: Total fuel consumption by time with the LA usage in the Charge Sustaining control strategy

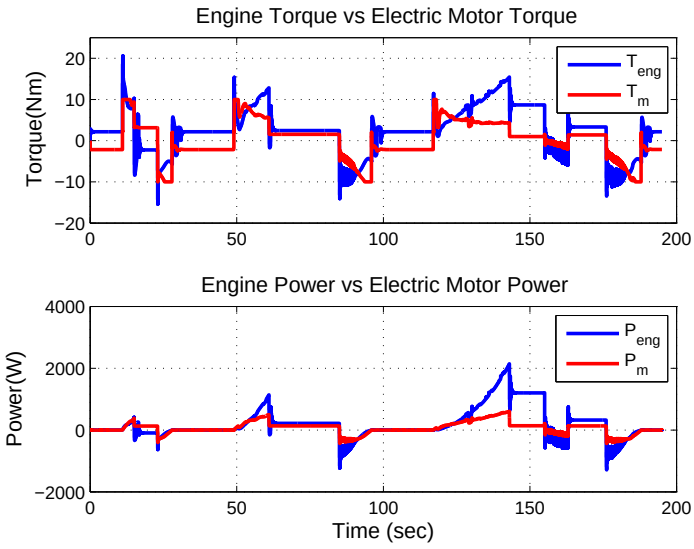

Figure 4.15: Motor and engine torque and power variations by time with the LA usage in the Charge Sustaining control strategy

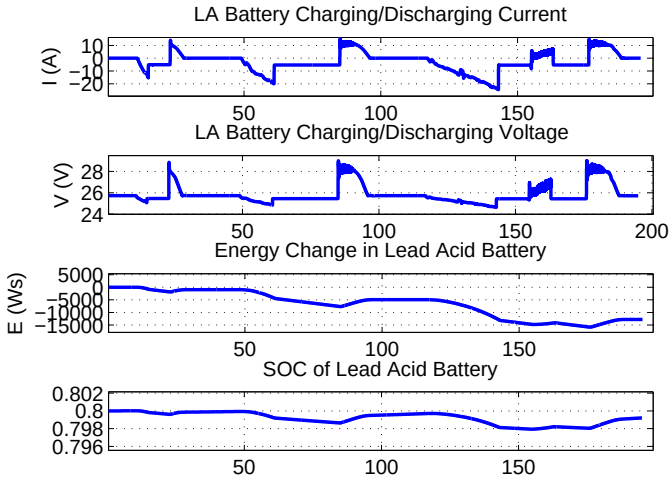

Figure 4.16: Lead acid battery current, voltage, energy and state of charge variations by time with the LA usage in the Charge Sustaining control strategy

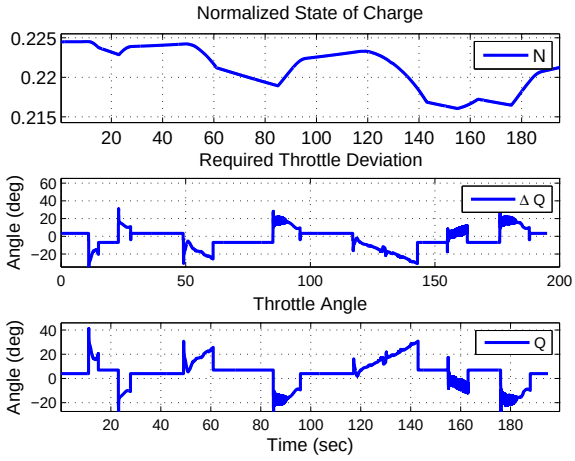

Figure 4.17: Normalized SOC, throttle angle deviation and throttle angle positions with the LA usage in the Charge Sustaining control strategy

While the vehicle engine consumes 49.6 kWs energy with the ultracapacitor storage module, vehicle engine consumes 46.6 kWs energy with the lead acid battery pack. During the time intervals of the electric motor assist, electric motor consumes 19.76 kWs with the ultracapacitor storage module, it consumes 25.5 kWs energy with the lead acid battery pack. In the regenerative breaking time intervals, while ultracapacitor package saves 7.28 kWs energy, lead acid battery saves 7.45 kWs. These results show that the usage of LA battery yields less fuel consumption with respect to the ultracapacitor module usage.

4.3 Optimal Control Strategy Simulation Results

During these simulations and experiments, hybrid karting vehicle's electric motor has been controlled with the control algorithm specified in section 3.4.2.3. In these simulations, vehicle follows the ECE15 driving cycle. Driver's input torque is calculated as described in the section 3.4.1 with a sliding mode controller. In a real scenario, driver input torque would be managed by the ICE through the throttle and brake pedals.

As it can be seen in figures 4.28 and 4.22, during acceleration time intervals current sign is negative which means charge is

depleting. During the deceleration time intervals, current sign becomes positive which means batteries are charging with the regenerative brake energy. Correspondingly, battery voltages and SOC levels are decreasing while battery charge is depleting, and increasing while battery is charging.

In this optimal control strategy, it is aimed that battery SOC level is protected at the end of the driving cycle while the fuel consumption minimization problem is solved. For maximum energy recuperation, engine functions as generator with its full torque. Moreover, motor boosts the engine power only during the acceleration time interval where the required power is above the average power.

4.3.1 Results with Ultracapacitor

In this part of the work, a 83F and 48V ultracapacitor module has been used. The reference speed given in figure 4.21 with the control of engine torque. The motor aids the traction torque which is controlled by optimal control strategy. The obtained motor torque can be seen in figure 4.29. During the speed-up/acceleration processes of the vehicle, electric motor generates positive torque. During the deceleration time intervals it

functions as a generator. As it can be seen in figure 4.28, final state of charge level is similar to the beginning of the driving range.

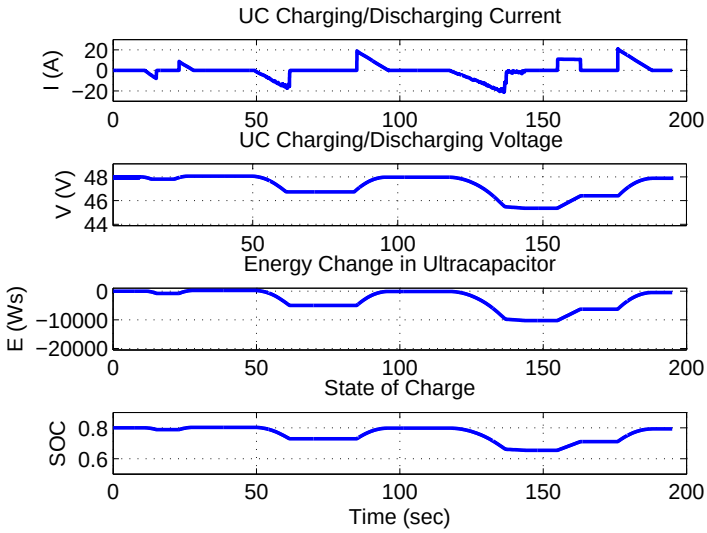

Figure 4.18: Battery current, voltage, energy and state of charge variations with UC usage in the Optimal Control strategy

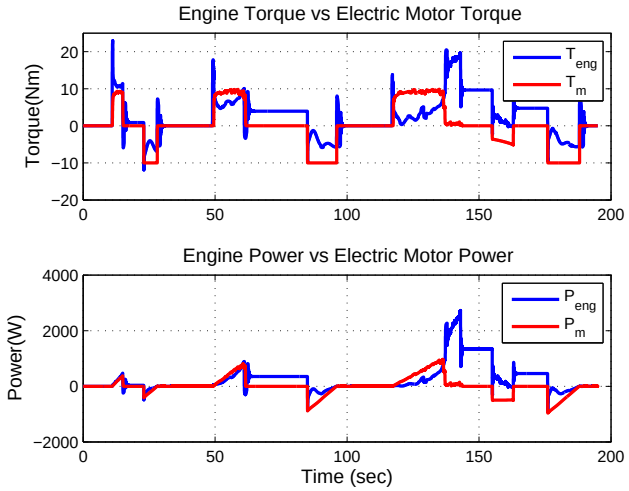

Figure 4.19: Motor and engine torque and power variations with UC usage in the Optimal Control strategy

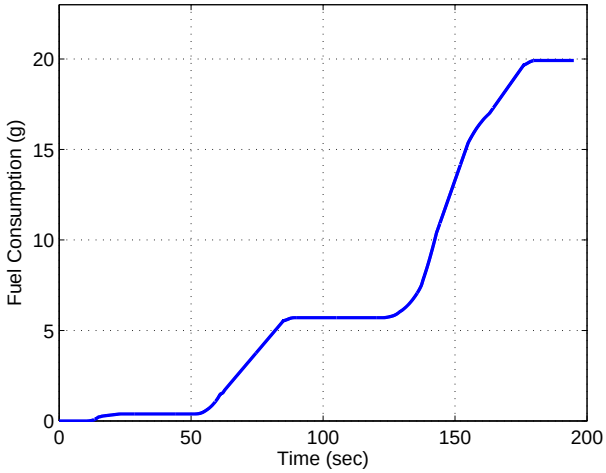

Figure 4.20: Total fuel consumption with UC usage in the Optimal Control strategy

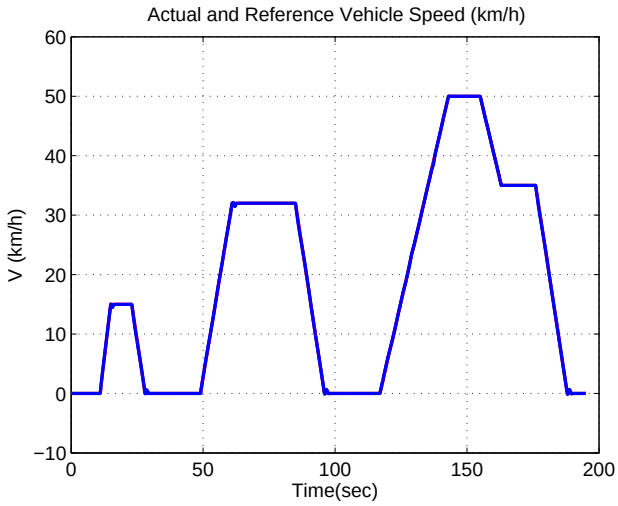

Figure 4.21: Reference speed and actual speed with Optimum Control

4.3.2 Results with Lead Acid Battery

In these simulations, lead acid car batteries have been used with 12V and 60Ah capacity. Two of them were connected in series as a battery package. The reference speed is given in figure 4.25 with the control of engine torque. The motor aids the traction torque which is controlled by optimal control strategy. The obtained motor torque can be seen in figure 4.23. During the speed-up/acceleration processes of the vehicle, electric motor boosts the engine power, and in the deceleration time intervals it functions as a generator.

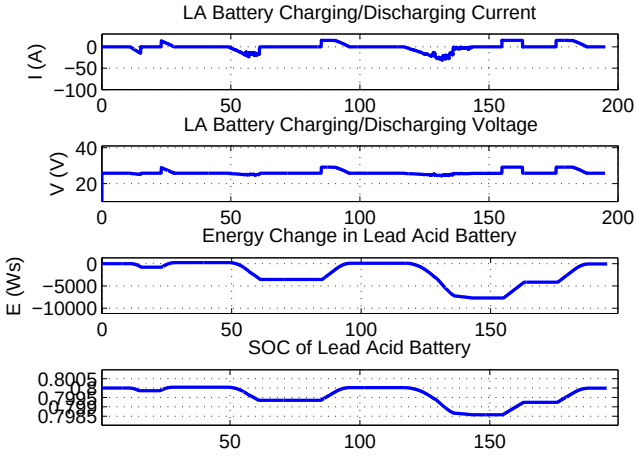

Figure 4.22: Battery current, voltage, energy and state of charge variations with LA battery usage in the Optimal Control strategy

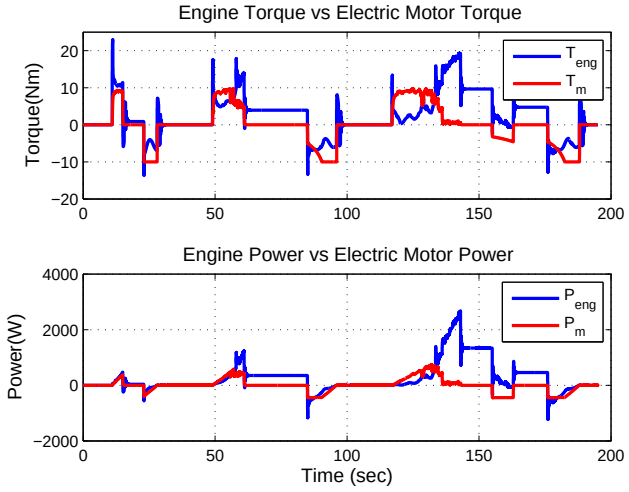

Figure 4.23: Motor and engine torque and power variations with LA battery usage in the Optimal Control strategy

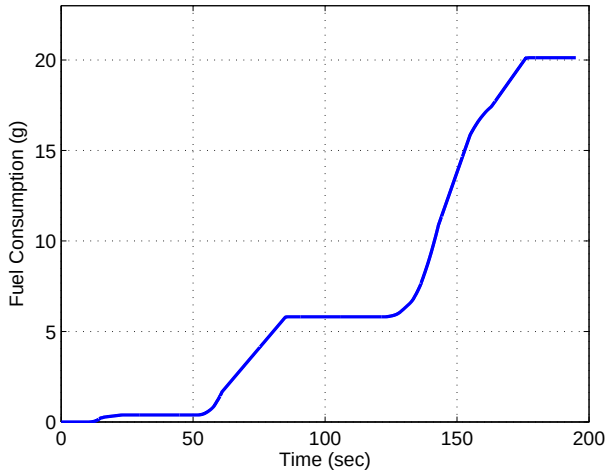

Figure 4.24: Total fuel consumption with LA battery usage in the Optimal Control strategy

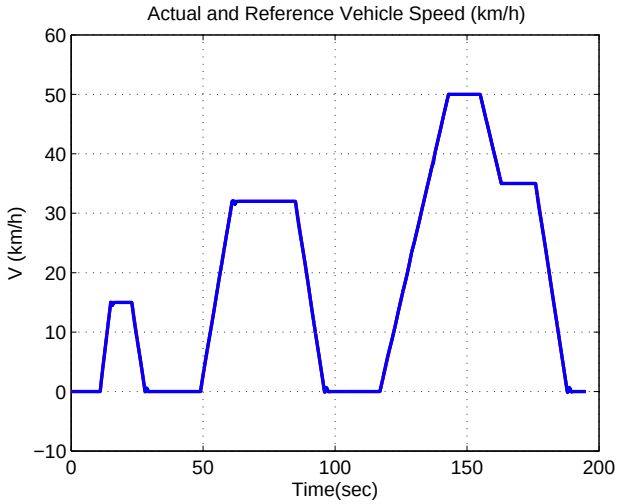

Figure 4.25: Reference speed and actual speed with Optimum Control

While the vehicle engine consumes 53.364 kWs energy with

the ultracapacitor storage module, vehicle engine consumes 56.89 kWs energy with the lead acid battery pack. During the time intervals of the electric motor assist, electric motor consumes 16.57 kWs with the ultracapacitor storage module, while it consumes 12.282 kWs energy with the lead acid battery pack. During regenerative breaking time intervals, while ultracapacitor package recuperates 16.02 kWs energy, lead acid battery saves 12.282 kWs.

In the optimal control problem, the usage of UC battery pack is important in terms of energy saving. Results show that %23.4 more energy is captured by the system with the use of ultracapacitor module.

4.4 Conventional Karting Vehicle Performance (without motor assist)

In this section, simulations have been performed in the absence of any battery and electric motor. It is aimed to see the required engine torque values and how much fuel is consumed to drive the karting vehicle in a given driving cycle.

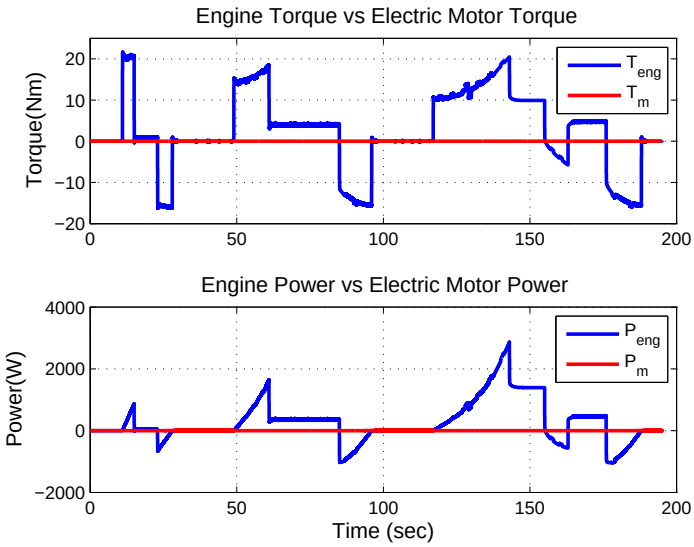

Figure 4.26: Motor and engine torque and power variations in the absence of electric motor

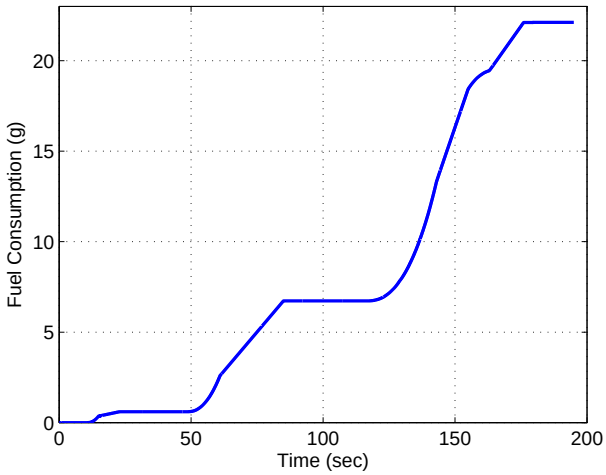

Figure 4.27: Total fuel consumption of engine in the absence of electric motor

It can be observed from the figure 4.27 that total fuel consumption to complete the ECE driving cycle is 22.12g. One can compare how much fuel is saved in the existence of electric motor by comparing the fuel consumption observed in section 4.1, 4.2 and 4.3. Furthermore, it is observed that engine reaches its maximum torque level around 21.59 Nm. It is calculated that the total energy required to drive the vehicle is 69,5 kWs in order to complete one ECE15 cycle.

4.5 Corrected Simulation After Experiments

During the experiments due to practical and physical limitations, some deviations from the estimated vs actual voltage levels have been observed. Details of these observations have been discussed later in the experimental work section. Based on the observations the simulation model has been corrected, and analyses have been repeated with reduced voltage levels. The results are presented as follows.

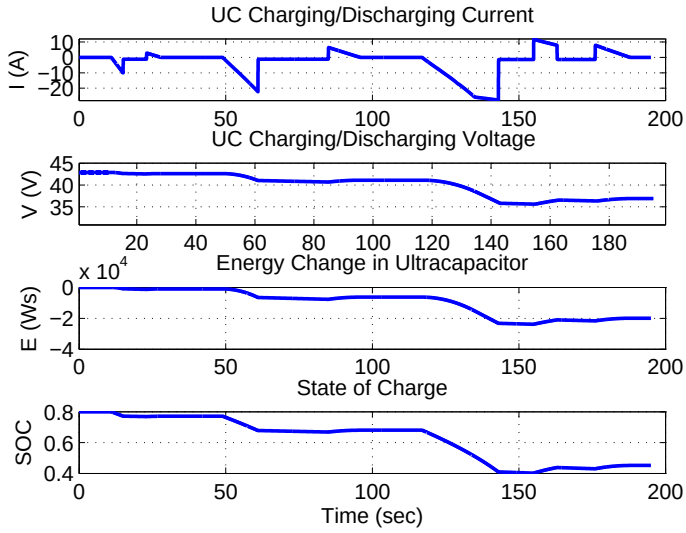

Figure 4.28: Battery current, voltage, energy and state of charge variations with UC usage in the Rule Based Control strategy

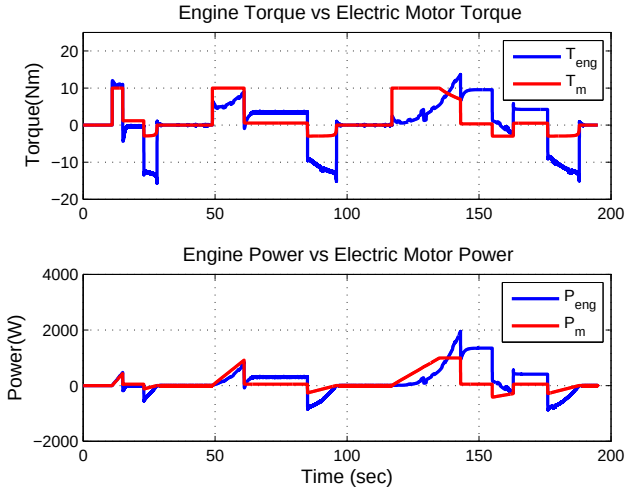

Figure 4.29: Motor and engine torque and power variations with UC usage in the Rule Based Control strategy

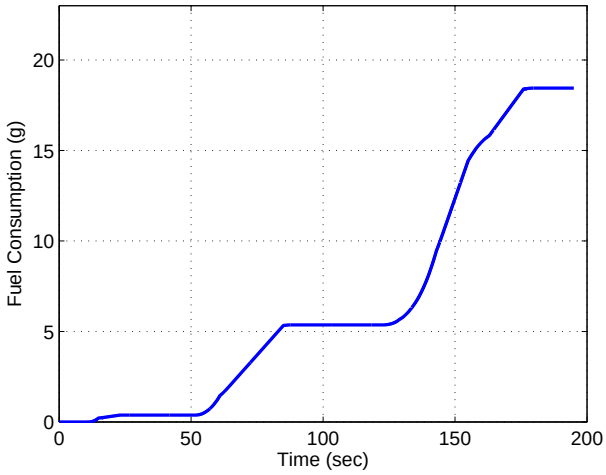

Figure 4.30: Total fuel consumption with UC usage in the Rule Based Control strategy

4.6 Discussion of Simulation Results

In this work, main aim is to achieve the maximum fuel saving. The simulation results showed that the maximum fuel saving can be achieved by the rule based controller by trading of the battery final SOC. Simulation results yield that maximum %35 fuel save can be obtained with the rule based controller while the recuperated energy is almost half of the used battery energy. In a real life application, the loss in stored energy should be compensated by charging from ICE during cruising times that may occur between typical simulated driving cycles.

Moreover, with the charge sustaining control algorithm, %28.63 fuel save is realized with the battery charge level trade off. Since the optimal control is strict on final SOC level, in order to protect the battery charge condition, less energy is consumed at the engine assist mode. It is observed that %23.74 is realized with the optimal control strategy.

While the rule based controller needs less computational effort, it has some disadvantages. All the road conditions may not be predicted beforehand. Therefore, rule based controller should be designed carefully. Even so, some problems may arise like unsustainable battery charge condition. It is observed that charge sustaining controller is creating problems in terms of controllability. Charge sustaining controller is sensitive to the pedal position which is creating problems in terms of electric motor controllability. Furthermore, optimal controller has high computational burden, since it requires pre-computation. In the optimal controller, SOC can be sustained with the constraints. However, optimal controller is not robust to system changes. Therefore, in order to use an optimal controller on a hybrid vehicle, an online-predictive controller should be developed. Besides, parameter tuning is harder than the other controllers.

Chapter V

5 Experimental Setup & Experimental Results

5.1 Laboratory Equipment

In order to test the simulation models and the performance of different storage systems in a laboratory environment, a test bench setup has been prepared with a Permanent Magnet DC motor and a servo-motor. The test bench setup can seen in figure 5.3

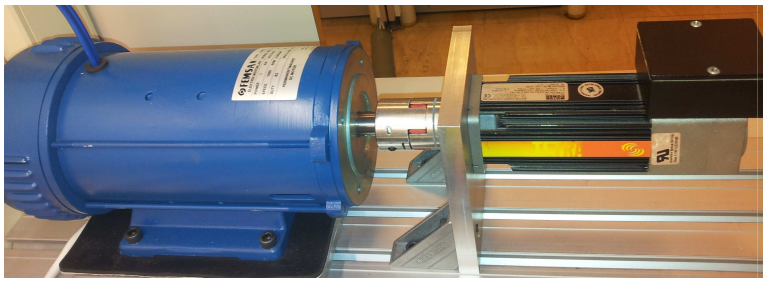

Figure 5.1: Test Bench Setup (right : DC Permanent Magnet Motor, left : Servo DC motor)

For the generator mode of the DC permanent motor, Servo motor was initially insufficient due to its low power capability. Therefore, another test-bench setup has been prepared as it can be seen in figure 5.2.

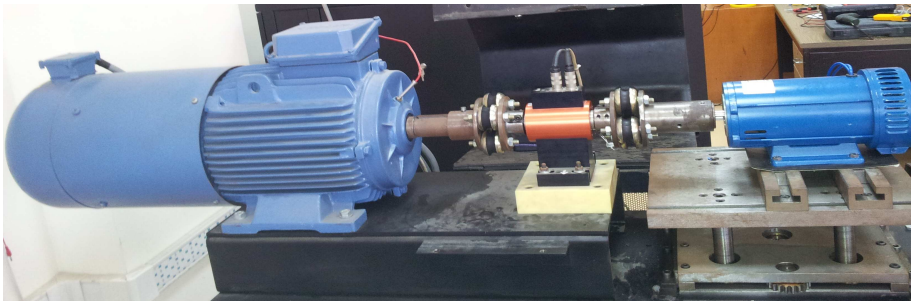

Figure 5.2: Test Bench Setup (right : 15 kW AC Motor, left : DC Permanent Magnet Motor)

5.1.1 Permanent Magnet DC Motor

As an electric motor, direct current (DC) permanent magnet (PM) motor has been selected. The PM DC motor uses permanent magnet to generate the magnetic field. This magnetic field rotates the armature. A FEMSAN 1 kW PM DC motor has been used. The motor properties are defined in table 5.1.

PM DC Motor Parameters	**Values**
Power	1 kW
Voltage	24 Volt
Current	48 A
Angular Velocity	1500 rpm
Torque Constant	0.1325 Nm/A
Back-EMF constant	0.1528 Vs/rad

Table 5.1: Permanent magnet DC motor characteristics

5.1.2 Battery/Storage Groups

In these experiments a 48V and 83F Maxwell ultracapacitor module and two 60Ah and 12V Varta car batteries have been used as storage elements.

Figure 5.3: 48V, 83F Maxwell Ultracapacitor Module

Figure 5.4: 60Ah, 12V Varta Car Battery

5.1.3 Voltage Acquisition

Voltage acquisition has been realized by NI USB-6009 low-cost multifunction data acquisition card (DAQ) which is 14-Bit and 48 kS/s. Properties of the data acquisition card can be found in table 5.2.

Figure 5.5: NI USB-6009

Properties	**Values**
Resolution	14 bits
Sample Rate	48 kS/s
Max. Voltage	10 V
Min. Voltage	-10 V
Voltage Range Accuracy	138 mV
Single Ended Channels	8

Table 5.2: NI USB-6009 Characteristics

5.1.4 Current Acquisition

Usually the hall current sensors measurements consist of high-frequency components, bursts and spikes, and a low frequency offset trend [48]. Hall effect sensor current measurement values can be described as in the following

$$I_{hallsensor}(t) = I_e + w(t) + I_{actual} \tag{1}$$

where I_e is the offset error, $w(t)$ is the white measurement noise and I_{actual} is the actual current value. As it can be observed from the figure 3.16, hall effect sensor noise is relatively high. Therefore, a smoothing filter is used.

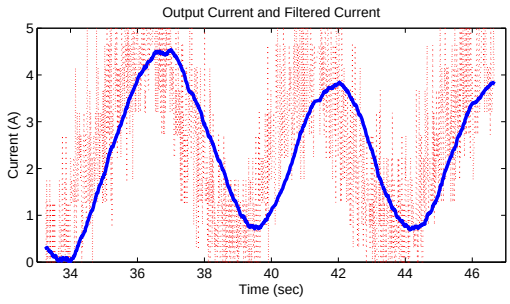

Figure 5.6: Hall effect sensor current value measurements and filtered current values

5.1.5 State of Charge Estimation Method

While some people prefer to use voltage method for state of charge estimations, this method is not very accurate, since the battery voltage value may show different values at different temperature intervals. Similarly, batteries may not show the correct voltage value with time. A more preferable method is coulomb counting method which uses current measurement.

State of charge can be defined as

$$SOC(t) = \frac{C_{nom} - \int_0^t I(t)\mathrm{d}t}{C_{nom}} \tag{2}$$

where $I(t)$ (A) is the battery current and C_{nom} is the battery nominal capacity. This definition is valid for fully charged batteries.

5.1.5.1 Coulomb Method

Coulomb counting method is the most preferable and simple way to get SOC information of battery. The problem with this method is the initial SOC of the battery can not be estimated. The coulomb counting method can be defined as in the following

$$SOC(t) = SOC(0) - \frac{\int_0^t I_m(t)\mathrm{d}t}{C_{nom}} \tag{3}$$

where $SOC(0)$ is the initial state of charge of the battery. However, it can not be measured without any prior knowledge. The noisy signal also creates problems with integration.

5.1.5.2 EMF voltage relationship with SOC

According to the Coleman et. al [49], there is a relationship between the electromotive voltage of the battery and the SOC of the battery as it is described in the following .

$$V_{EMF} = \alpha \cdot SOC + V_{EMF\_min} \tag{4}$$

Therefore, one can calculate the state of the charge of the battery as in the following

$$SOC = \frac{V_{EMF} - V_{EMF\_min}}{\alpha} \tag{5}$$

where V_{EMF} is the electromotive force which is the battery open circuit voltage when the battery in equilibrium or in open circuit for a long period of time. α is the slope of EMF voltage change with SOC.

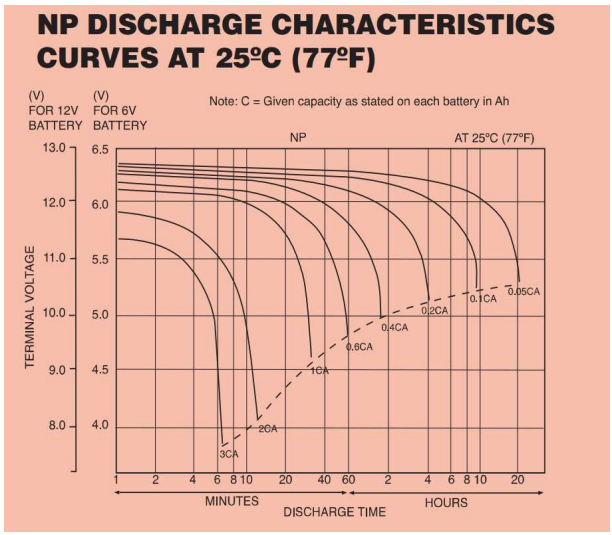

Figure 5.7: Current value measurement of hall effect sensor and filtered current values [50]

We can compensate the deficiency of the coulomb method SOC estimation by calculating the initial SOC of the battery by using the relationship between electromotive voltage and SOC.

5.2 Experiment Work

Experimental set-up can be visualized as in the figure 5.10. While the Motor:1 is standing for the engine and the vehicle load, Motor:2 is standing for the electric motor of the hybrid karting vehicle.

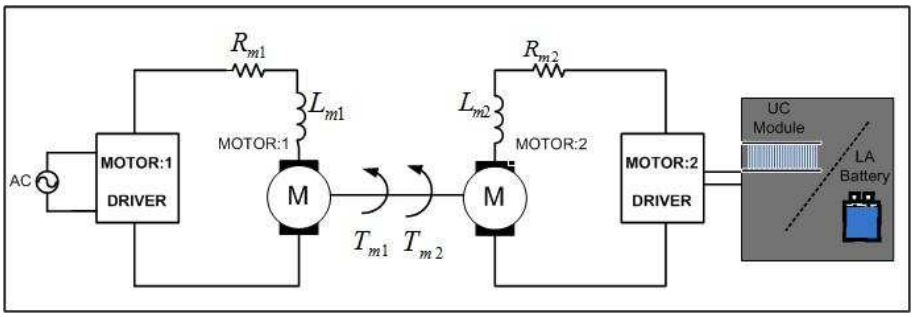

Figure 5.8: Test Bench Setup Visualization

5.2.1 Acceleration Tests

In acceleration mode of the karting vehicle, PM DC motor is in the power assisting mode where it is is sharing the driving torque of the vehicle. The tests have been conducted such that Motor No.2 (PM DC motor) is accelerating the shaft while the Motor No.1 (AC motor) is loading the shaft in order to match the motor torque during experiments. In simulations, motor torque has been represented with T_m. In experimental setup, Motor No.2 takes this role, and its torque is represented with T_{m2}. Motor No.2 torque is set similar to that of the motor torque of the karting vehicle.

$$T_{m2} = T_m \tag{6}$$

In short, Motor No.2 is accelerating the shaft against the resisting torque of Motor No.1 which represents inertia loads.

$$T_{m2} = J_{total}\alpha + T_{m1} \tag{7}$$

where J_{total} is equal to total inertia of the shaft such that

$$J_{total} = J_{m1} + J_{m2} \tag{8}$$

From the experiments it is calculated that the total inertia of the shaft is 0.4255 kgm^2.

5.2.2 Deceleration Tests

In the deceleration time intervals of the vehicle, electrical motor is functioning as generator. While Motor No.1 simulates car and system loads in accordance with the driving cycle deceleration rate, Motor No.2 functions as generator and applies resisting torque to the system. One can calculate how much torque should be applied by the Motor No.1 to follow the deceleration profile of the driving cycle, as it is described in the following.

$$T_{m1} = J\alpha - T_{m2} \tag{9}$$

Motor No.2 torque is calculated with the current measurement I_{m2} as in the following

$$T_{m2} = k_{t2} I_{m2} \tag{10}$$

Torque sensor measurement gives one the total torque due to Motor.No1 and Motor.No2.

$$T_{sensor} = T_{m1} + T_{m2} \tag{11}$$

In the generation mode of the Motor.No2, motor voltage can be described with the following formula.

$$E_{m2} = k_{m2} i_{m2} \tag{12}$$

where k_{m1} is the back-EMF (torque) constant. Motor generated voltage is proportional to the shaft velocity. This voltage can be described with the system dynamics as in the following

$$k_{m2} w = L_{m2} \frac{di_{m2}}{dt} + (R_{m2} + R_{batt}) i_{m2} \tag{13}$$

5.3 Experiment Results

In this section experiments have been conducted with the rule based controller with the lead acid battery and ultracapacitor one by one.

5.3.1 Experiment Results with Lead Acid Battery Package

It is observed that in the rule based control, while 25.6 kWs energy is discharged from the battery, 3.6 kWs energy is charged in the generation mode of the motor. As it can be seen from the figure 5.10, battery charge current is reaching its top value 13.46A at the maximum speed value of the driving cycle angular velocity of 1326rpm.

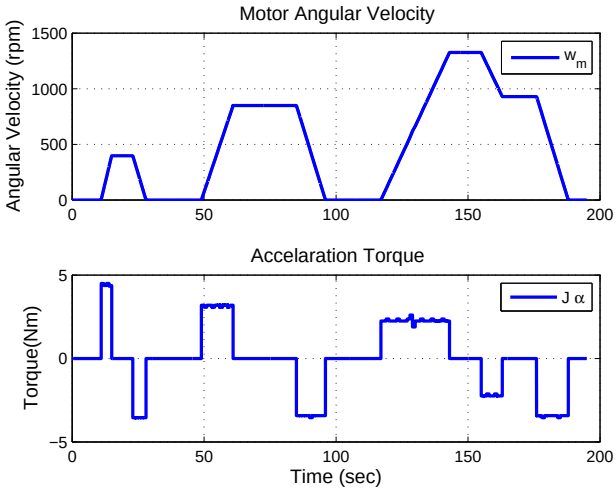

Figure 5.9: Motor.No2 Angular velocity profile and required acceleration torque graphics.

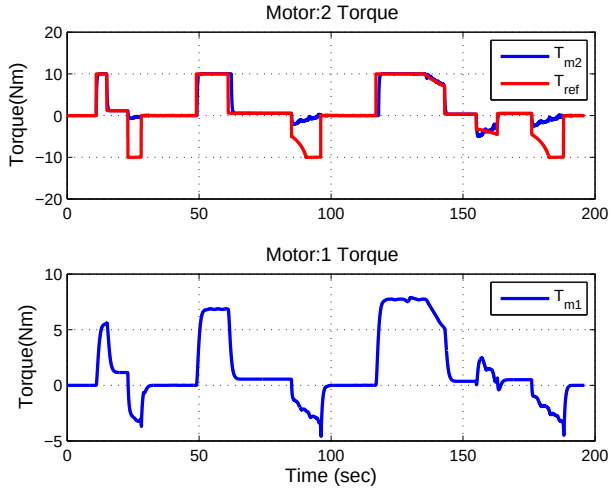

Figure 5.10: LA battery current and its state of charge change by time.

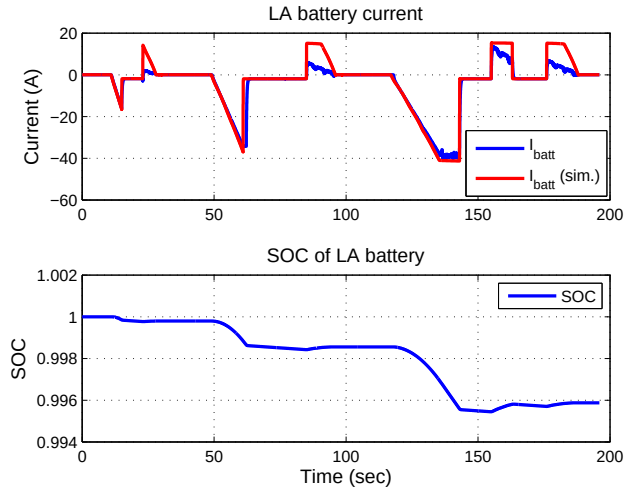

Figure 5.11: Motor.No2 reference torque (red) and its actual torque (blue), and Motor:1 followed torque in experiment

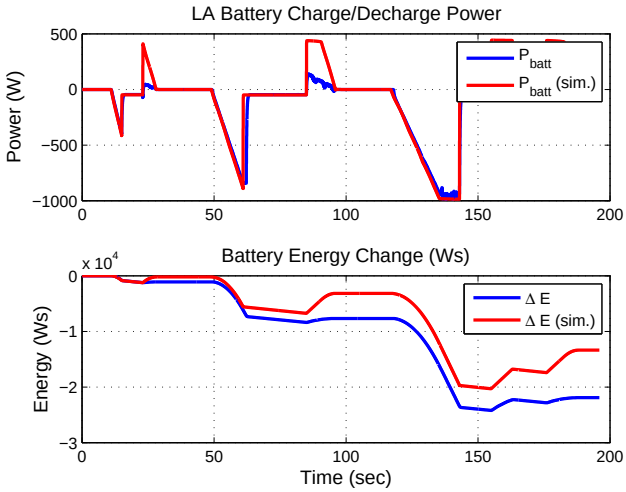

Figure 5.12: LA battery power in experiment (blue) and LA battery power in simulations (red), and energy change of LA battery by time in experiment (blue) and in simulation (red)

5.3.2 Experiment Results with Ultracapacitor Package

It is observed that in the rule based control, while 27.2 kWs energy is discharged from the ultracapacitor package, ultracapacitor is charged with the 4.6 kWs energy in the generation mode of the motor. As it can be seen from the figure 5.10, battery charge current is reaching its top value of 13.56A at the maximum speed value of the driving cycle angular velocity of 1326rpm.

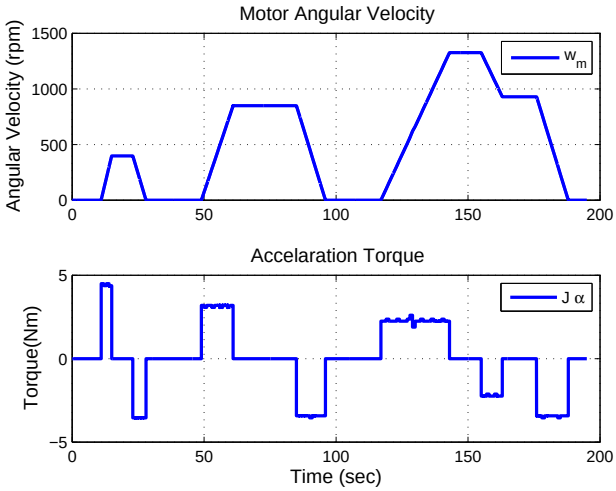

Figure 5.13: Motor.No2 Angular velocity profile and required acceleration torque graphics.

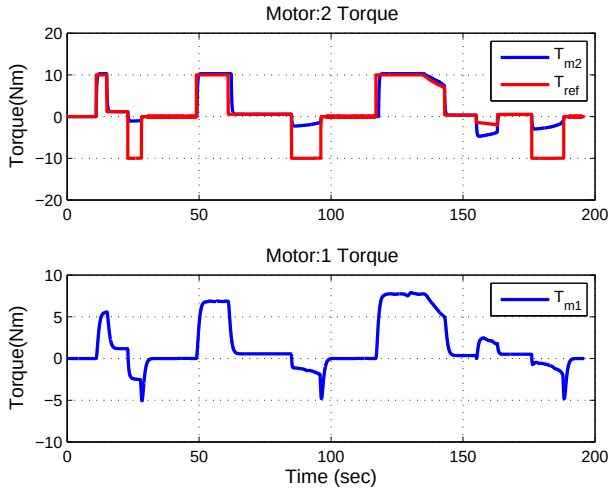

Figure 5.14: UC current and its state of charge change by time.

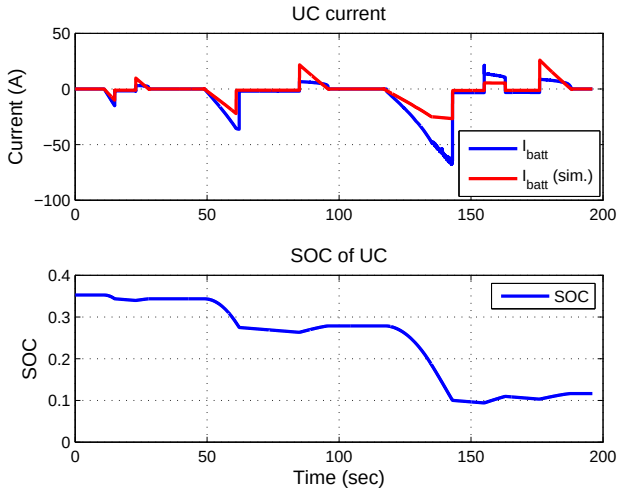

Figure 5.15: Motor.No2 reference torque (red) and its actual torque (blue), and Motor:1 followed torque in experiment

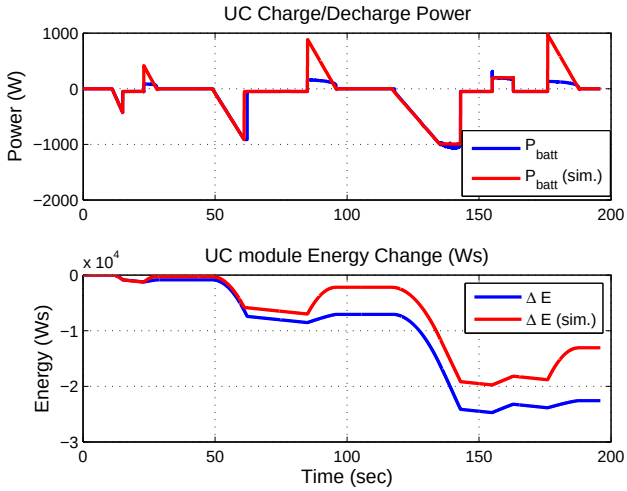

Figure 5.16: UC power in experiment (blue) and UC power in simulations (red), and energy change of UC by time in experiment (blue) and in simulation (red)

- Experimental result and simulation results comparison after correction in simulation environment

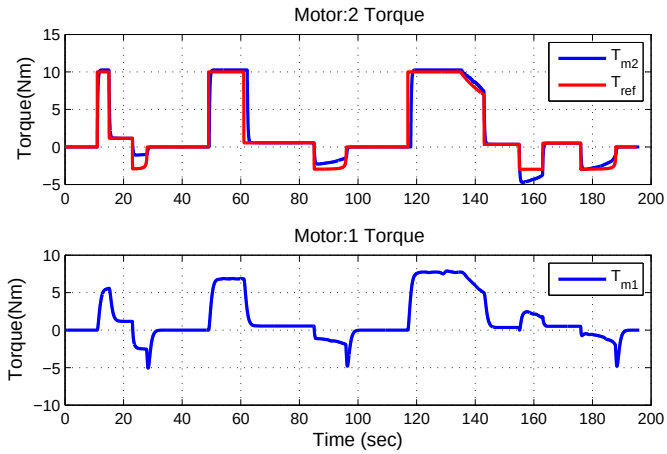

Figure 5.17: Motor.No2 reference torque (red) and its actual torque (blue), and Motor:1 followed torque in experiment

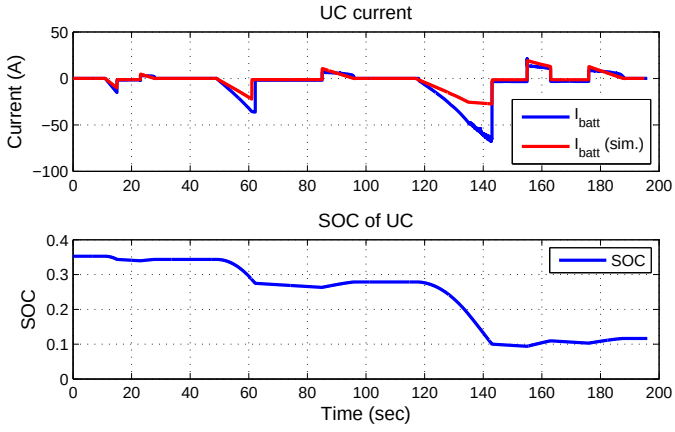

Figure 5.18: UC current and its state of charge change by time.

5.4 Comparison of Simulation and Experimental Results

As it can be observed from figure 4.1, ultracapacitor voltage is started from the 42.93V which corresponds to battery SOC of 80%. On the other side, hardware restriction limited the working range of ultracapacitor module. While the PM DC motor driver's working range is 18V to 48V, this range is restricted by the manufacturer in the voltage interval of 18.5V to 28.5V. Therefore, experimental results show differences in terms of UC SOC level and working voltage range as it can be seen in figure 5.14. In the experiments, beginning UC voltage is 28.5V which corresponds to %35 SOC level and at the end of the driving cycle its voltage drops to 16.44V which corresponds to %11.64 SOC level of the battery. Working in high voltage level of ultracapacitor is advantageous, since its capacity is proportional to square of its voltage.

Working voltage interval also effected the battery charge and discharge current values, since the required power is product of battery voltage and its current, lower voltage working range leads to higher current levels.

The difference between the experiments and the simulation

is the generating power. The simulations that were conducted before the experiments, assumed the supply of full torque in the generation mode. After the experiments, a generator model has been integrated to the model, with changing generation energy.

Chapter VI

6 Conclusion & Future Works

In this study, a model is developed for a hybrid karting vehicle which is converted to hybrid from an conventional vehicle. The conversion is achieved by integrating an electric motor to the shaft of the IC engine. A power storage module is added in order to boost the engine power during acceleration and to recapture the kinetic energy of the vehicle during breaking.

In order to develop an efficient control methodology for the electric motor control during the driving range, a model is needed in simulation environment. A mathematical model is developed using Simulink/Matlab with the Simscape/Mechanical library. A lead acid battery pack and ultracapacitor module are integrated into the model. Battery models are developed considering charging and discharging resistances for different temperatures.

In order to find the best controller for the hybrid vehicle control model algorithms are developed with three different con-

trollers. First, a rule based control algorithm which is based on vehicle speed and battery SOC condition is developed. Then, a charge sustaining control algorithm is developed in order to evaluate the system efficiency while the charge is sustained. Finally, an optimal controller is developed in order to make the engine work at its efficient regions while the battery SOC is protected at the end of its driving range.

After the control algorithms are developed, system is tested at a test bench. The experimental study has showed that lead acid batteries can be used in hybrid karting vehicles. Lead acid batteries can stand to high current rates during discharging processes with 2C rate. However, their charging current limits are limited with 0.25-0.3C rate. On the other side, ultracapacitors can stand to both high charging and discharging rates. Since regenerative break energy requires immediate energy conversion, ultracapacitors play an important role in energy conversion process with their high current rate capabilities. The results indicate that for minimal fuel consumption one should prefer ultracapacitors by trading off the price.

As future work, control scenarios can be implemented to a hybrid karting car road test. For this implementation, a hybrid

control unit and engine control unit will be required as shown in the figure 6.1. Hybrid control unit will be responsible of the management of the electric motor under changing conditions. For the driveline management, it is required to know the the pedal position and vehicle actual speed. Battery temperature and its state of charge knowledge should be under control to prevent any damage to them.

Power consumption can be optimized with integration of optimization algorithms into the rule based algorithm. In order to put the optimal controller on a real driving case, online optimization method should be developed with the predicted road conditions.

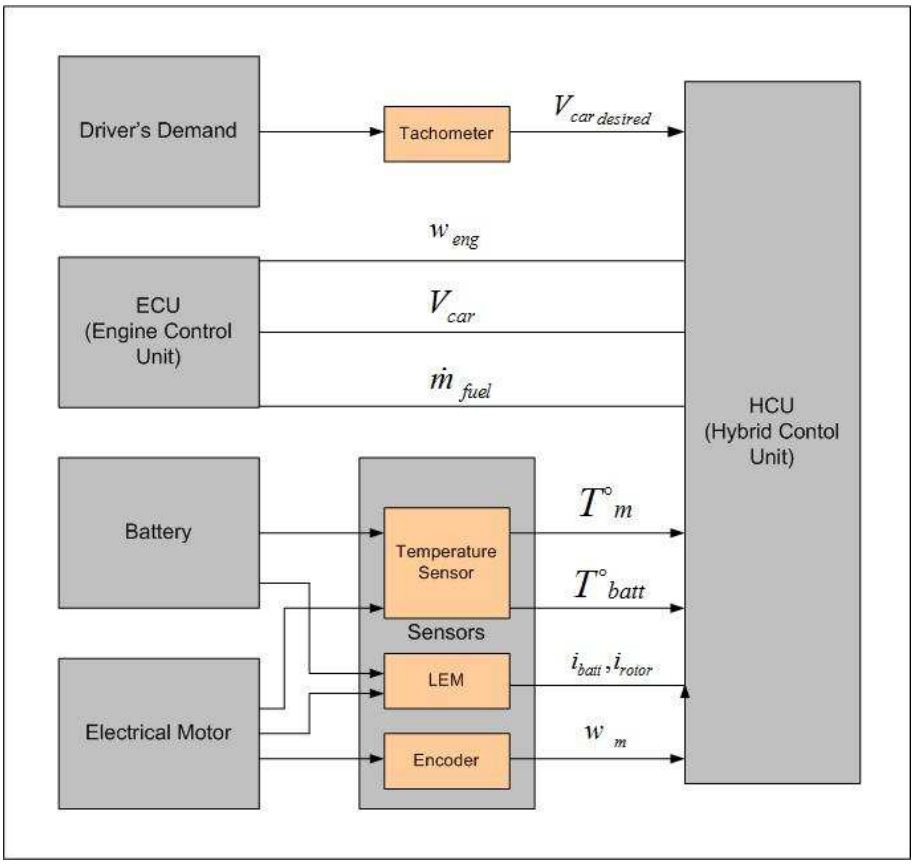

Figure 6.1: Hybrid karting car management units communication.

References

[1] *TTC going diesel again after hybrid bus glitch*, thestar.com/News/GTA/article/519770, 13 Feb. 2012.

[2] *Toplu Tasima Araclari*, iett.gov.tr/metin.php?no=16, 14 Feb. 2012.

[3] Jinming Liu; Huei Peng; , *Modeling and Control of a Power-Split Hybrid Vehicle,* IEEE Transactions on Control Systems Technology, vol.16, no.6, pp.1242-1251, Nov. 2008.

[4] P. Tulpule, V. Marano, G. Rizzoni, *Effects of different PHEV control strategies on vehicle performance*, American Control Conference, 2009. ACC '09. , vol., no., pp.3950-3955, 10-12 June 2009.

[5] Aso, S.; Kizaki, M.; Nonobe, Y., *Development of Fuel Cell Hybrid Vehicles in TOYOTA*, Power Conversion Conference - Nagoya, 2007. PCC '07 , pp.1606-1611, 2-5 April 2007.

[6] *Ohio Electric Motors:Permanent Magnet DC Motors* www.ohioelectricmotors.com/permanent-magnet-dc-motors-649ixzz22uER4uAQ.

[7] Miller, J.; McCleer P. J.; Cohen M., *Energy Buffers*, Maxwell Technologies White Paper.

[8] Besnier, F.; Sharer, P; Monnet, G.; Rousseau A., *Dual Source Energy Storage Potential for Fuel Cell Vehicle Applications*, Argonne National Laboratory.

[9] Baisden, A.C.; Emadi, A.; , *ADVISOR-based model of a battery and an ultra-capacitor energy source for hybrid electric vehicles*, Vehicular Technology, vol.53, no.1, pp. 199-205, Jan. 2004.

[10] Di Napoli, A.; Crescimbini, F.; Solero, L.; Caricchi, F.; Capponi, F.G.; , *Multiple-input DC-DC power converter for power-flow management in hybrid vehicles*, Industry Applications Conference, 2002. 37th IAS Annual Meeting. Conference Record of the, vol.3, no., pp.1578-1585 vol.3, 13-18 Oct. 2002.

[11] Lukic, S.M.; Wirasingha, S.G.; Rodriguez, F.; Jian Cao; Emadi, A.; , "Power Management of an Ultracapacitor/Battery Hybrid Energy Storage System in an HEV," Vehicle Power and Propulsion Conference, 2006. VPPC '06. IEEE, pp.1-6, 6-8 Sept. 2006.

[12] Garcia, F.S.; Ferreira, A.A.; Pomilio, J.A. , *Control Strategy for Battery-Ultracapacitor Hybrid Energy Storage System*, Applied Power Electronics Conference and Exposition, 2009. APEC 2009. Twenty-Fourth Annual IEEE, pp.826-832, 15-19 Feb. 2009.

[13] Miller, J.; McCleer P. J.; Cohen M., *Energy Buffers*, Maxwell Technologies White Paper.

[14] B. Zhang, C.C. Mi, T.M. M. Zhang, *Charge-Depleting Control Strategies and Fuel Optimization of Blended-Mode Plug-In Hybrid Electric Vehicles*, IEEE Transactions on Vehicular Technology, vol.60, no.4, pp.1516-1525, May 2011.

[15] Besnier, F.; Sharer, P; Monnet, G.; Rousseau A., *Dual Source Energy Storage Potential for Fuel Cell Vehicle Applications*, Argonne National Laboratory.

[16] Stienecker, A.W.; Stuart, T.; Ashtiani, C. , *A combined ultracapacitor-lead acid battery storage system for mild hybrid electric vehicles,* Vehicle Power and Propulsion, 2005 IEEE Conference , pp. 6 pp., 7-9 Sept. 2005.

[17] Baisden, A.C.; Emadi, A.; , *ADVISOR-based model of a battery and an ultra-capacitor energy source for hybrid elec-*

tric vehicles, Vehicular Technology, vol.53, no.1, pp. 199-205, Jan. 2004.

[18] Di Napoli, A.; Crescimbini, F.; Solero, L.; Caricchi, F.; Capponi, F.G.; , *Multiple-input DC-DC power converter for power-flow management in hybrid vehicles*, Industry Applications Conference, 2002. 37th IAS Annual Meeting. Conference Record of the, vol.3, no., pp.1578-1585 vol.3, 13-18 Oct. 2002.

[19] Lukic, S.M.; Wirasingha, S.G.; Rodriguez, F.; Jian Cao; Emadi, A.; , "Power Management of an Ultracapacitor/Battery Hybrid Energy Storage System in an HEV," Vehicle Power and Propulsion Conference, 2006. VPPC '06. IEEE, pp.1-6, 6-8 Sept. 2006.

[20] Garcia, F.S.; Ferreira, A.A.; Pomilio, J.A. , *Control Strategy for Battery-Ultracapacitor Hybrid Energy Storage System*, Applied Power Electronics Conference and Exposition, 2009. APEC 2009. Twenty-Fourth Annual IEEE, pp.826-832, 15-19 Feb. 2009.

[21] C. Desai, S.S. Williamson, *Comparative study of hybrid electric vehicle control strategies for improved drivetrain ef-*

ficiency analysis,Electrical Power and Energy Conference (EPEC), 2009 IEEE, pp.1-6, 22-23 Oct. 2009.

[22] Y. Zhang, H. Lin, B. Zhang, C. Mi, *Performance modelling and optimization of a novel multi mode hybrid powertrain*, Trans. ASME, J. Mech. Design,2006, 128(1), pp. 79-89.

[23] B. Zhang, C.C. Mi, T.M. M. Zhang, *Charge-Depleting Control Strategies and Fuel Optimization of Blended-Mode Plug-In Hybrid Electric Vehicles*, IEEE Transactions on Vehicular Technology, vol.60, no.4, pp.1516-1525, May 2011.

[24] Jong-Seob Won; Langari, R.; Ehsani, M. , *An energy management and charge sustaining strategy for a parallel hybrid vehicle with CVT,* IEEE Transactions on Control Systems Technology, vol.13, no.2, pp. 313- 320, March 2005.

[25] F.U. Syed, M.L. Kuang, J. Czubay, J.; H. Ying *Derivation and Experimental Validation of a Power-Split Hybrid Electric Vehicle Model*, IEEE Transactions on Vehicular Technology, vol.55, no.6, pp.1731-1747, Nov. 2006

[26] Tian Yi; Zhang Xin; Zhang Liang; *Fuzzy-Genetic Control Strategy of Hybrid Electric Vehicle*, Intelligent Computation

Technology and Automation, 2009. ICICTA '09. Second International Conference on , vol.2, no., pp.720-723, 10-11 Oct. 2009.

[27] Hyeoun-Dong Lee; Euh-Suh Koo; Seung-Ki Sul; Joohn-Sheok Kim; Kamiya, M.; Ikeda, H.; Shinohara, S.; Yoshida, H.; , *Torque control strategy for a parallel-hybrid vehicle using fuzzy logic,* Industry Applications Magazine, IEEE , vol.6, no.6, pp. 33- 38, Nov-Dec 2000.

[28] Wang Yifeng; Zhang Yun; Wu Jian; Chen Ning; , *Energy management system based on fuzzy control approach for hybrid electric vehicle,* Control and Decision Conference, 2009. CCDC '09. Chinese , vol., no., pp.3382-3386, 17-19 June 2009.

[29] Gokasan, M.; Bogosyan, S.; Goering, D.J.; , *Sliding mode based powertrain control for efficiency improvement in series hybrid-electric vehicles*, Power Electronics, IEEE Transactions on , vol.21, no.3, pp.779-790, May 2006.

[30] Demirci, M.; Biliroglu, A.O.; Go¨kasan, M.; Bogosyan, S.; , *Sliding mode optimum control for APU of series hybrid*

electric vehicles, 2010 IEEE International Symposium on Industrial Electronics (ISIE), pp.340-345, 4-7 July 2010.

[31] Xudong Wang; Ningzhi Jin; Hanying Gao; Hesong Cui; , *Sliding mode based MTPA control system of IPMSM for hybrid electrical vehicles*, Strategic Technology (IFOST), 2011 6th International Forum on , vol.1, no., pp.295-299, 22-24 Aug. 2011.

[32] Yaonan Wang; Xizheng Zhang; Xiaofang Yuan; Guorong Liu; , *Position-Sensorless Hybrid Sliding-Mode Control of Electric Vehicles With Brushless DC Motor*, IEEE Transactions on Vehicular Technology, vol.60, no.2, pp.421-432, Feb. 2011.

[33] Hong Fu; Guangyu Tian; Yaobin Chen; Quanshi Chen; , "Sliding mode-based DTC-SVM control of permanent magnet synchronous motors for plug-in hybrid electric vehicles," Vehicle Power and Propulsion Conference, 2009. VPPC '09. IEEE, pp.500-505, 7-10 Sept. 2009.

[34] Tian-Jun Fu; Wen-Fang Xie; , *Torque control of induction motors for hybrid electric vehicles*, American Control Conference, 2006 , vol., no., pp.6 pp., 14-16 June 2006.

[35] Fazeli, A.; Zeinali, M.; Khajepour, A.; , *Application of Adaptive Sliding Mode Control for Regenerative Braking Torque Control*, Mechatronics, IEEE/ASME Transactions on , vol.PP, no.99, pp.1-11, 0.

[36] Jeongyun Cheong; Wesub Eom; Jangmyung Lee; , *Cornering stability improvement for 4 wheel drive hybrid electric vehicle*, Industrial Electronics, 2009. ISIE 2009. IEEE International Symposium on , vol., no., pp.853-858, 5-8 July 2009.

[37] Taghavipour, A.; Alasty, A.; Saadat, M.F.; , *Nonlinear Power Balance Control of a SPA hydraulic hybrid truck*, Advanced Intelligent Mechatronics, 2009. AIM 2009. IEEE/ASME International Conference on , vol., no., pp.805-810, 14-17 July 2009.

[38] Zidani, F.; Benbouzid, M.E.H.; Diallo, D.; Benchaib, A.; , *Active fault-tolerant control of induction motor drives in EV and HEV against sensor failures using a fuzzy decision system*, Electric Machines and Drives Conference, 2003. IEMDC'03. IEEE International , vol.2, no., pp. 677- 683 vol.2, 1-4 June 2003.

[39] Kasahara, M.; Kanai, Y.; Mori, Y.; , *Vehicle braking control using sliding mode control - Switching control for speed and slip ratio*, ICCAS-SICE, 2009 , vol., no., pp.4047-4052, 18-21 Aug. 2009.

[40] C. Desai, S.S. Williamson, *Comparative study of hybrid electric vehicle control strategies for improved drivetrain efficiency analysis*,Electrical Power and Energy Conference (EPEC), 2009 IEEE, pp.1-6, 22-23 Oct. 2009.

[41] S. Stockar, V. Marano, G. Rizzoni and L. Guzzella L. *Energy-Optimal Control of Plug-in Hybrid Electric Vehicles for Real-World Driving Cycles*, IEEE Transactions on Vehicular Technology, vol.60, no.7, pp.2949-2962, Sept. 2011.

[42] S. Delprat, J. Lauber, T.M. Guerra, J. Rimaux, *Control of a parallel hybrid powertrain: optimal control*, IEEE Transactions on Vehicular Technology, vol.53, no.3, pp. 872- 881, May 2004.

[43] D. V. Ngo, T. Hofman, M. Steinbuch, A.F.A. Serrarens, *An optimal control-based algorithm for Hybrid Electric Vehicle using preview route information*, American Control Conference (ACC), 2010, pp.5818-5823, June 30 2010-July 2 2010.

[44] M. Huang, *Optimal Multilevel Hierarchical Control Strategy for Parallel Hybrid Electric Vehicle*, Vehicle Power and Propulsion Conference, 2006. VPPC '06. IEEE, pp.1-4, 6-8 Sept. 2006.

[45] A. Sciarretta, M. Back and L. Guzzella, *Optimal control of parallel hybrid electric vehicles*, Control Systems Technology, IEEE Transactions on , vol.12, no.3, pp. 352- 363, May 2004.

[46] Menyang Zhang; Yan Yang; Mi, C.C., *Analytical Approach for the Power Management of Blended-Mode Plug-In Hybrid Electric Vehicles*, IEEE Transactions on Vehicular Technology , vol.61, no.4, pp.1554-1566, May 2012.

[47] Jackey, R.A. ; Chi Kwan Lee; Chunbo Zhu; Hurley, W.G.; , *A Simple, Effective Lead-Acid Battery Modeling Process for Electrical System Component Selection,* The Mathworks, Inc.

[48] Portas, R.; Colombel L., *Accuracy of Hall-Effect Current Measurement Transducers in Automotive Battery Management Applications using Current Integration,* Automotive Power Electronics, Sep. 2007.

[49] Coleman, M.; Chi Kwan Lee; Chunbo Zhu; Hurley, W.G.; , *State-of-Charge Determination From EMF Voltage Estimation: Using Impedance, Terminal Voltage, and Current for Lead-Acid and Lithium-Ion Batteries,* Industrial Electronics, IEEE Transactions on , vol.54, no.5, pp.2550-2557, Oct. 2007.

[50] *Datasheet of NP7-12* aetes.com/YUASA/pdf/. 08 Aug, 2012.